**NTNU – Trondheim**
Norwegian University of
Science and Technology

# Modelling of Adaptive Geometry Flow Control Solutions in CFD

## Anne Vea

# NTNU

Norwegian University
of Science and Technology
NTNU

Department of Energy
and Process Engineering

EPT-M-2012-88

## MASTER THESIS

for

Stud.techn. Anne Vea
Spring 2012

### *Modeling of adaptive geometry flow control solutions in CFD*
*Modellering i CFD av adaptiv geometri for bruk i flow control løsninger*

**Background and objective.**

Flow Control is here defined as the collection of techniques that improves off-design performance, or reduced deleterious effects, in fluid flow system but with a minimum influence on the over-all functionality of the system where said technique is deployed.

One line of flow control is the use of (dynamically) adaptive surfaces to morph the fluid flow system toward a geometry configuration that is more fit to the instantaneous operating mode. Typically such techniques could be applied in wind-turbines/ airplane wings and in stationary cascades of hydro turbines. The actual speed of geometry adaption is limited by added mass effects, and the objective of this work is to explore these limitations.

**The following questions should be considered in the project work:**

1 A literature study establishing state of the art shall be made. Special attention should be given added mass effects.
2 The use of CFD shall be applied to demonstrate dynamic geometry adaption and/or added mass effects in fluid flows. The demonstration should either use (1) Moving mesh on a oscillating bluff body, (2) Deforming mesh on an oscillating beam in fluid flow, (3) Deformable proturbances on cylinder or (4) a system suggested by the candidate.
3 Discussion on technologies to increase speed of adaptive geometries; e.g. auto-tuning mecahnical resonance systems.

-- ” --

Within 14 days of receiving the written text on the diploma thesis, the candidate shall submit a research plan for his project to the department.

When the thesis is evaluated, emphasis is put on processing of the results, and that they are presented in tabular and/or graphic form in a clear manner, and that they are analyzed carefully.

The thesis should be formulated as a research report with summary both in English and Norwegian, conclusion, literature references, table of contents etc. During the preparation of the text, the candidate should make an effort to produce a well-structured and easily readable report. In order to ease the evaluation of the thesis, it is important that the cross-references are correct. In the making of the report, strong emphasis should be placed on both a thorough discussion of the results and an orderly presentation.

The candidate is requested to initiate and keep close contact with his/her academic supervisor(s) throughout the working period. The candidate must follow the rules and regulations of NTNU as well as passive directions given by the Department of Energy and Process Engineering.

Risk assessment of the candidate's work shall be carried out according to the department's procedures. The risk assessment must be documented and included as part of the final report. Events related to the candidate's work adversely affecting the health, safety or security, must be documented and included as part of the final report.

Pursuant to "Regulations concerning the supplementary provisions to the technology study program/Master of Science" at NTNU §20, the Department reserves the permission to utilize all the results and data for teaching and research purposes as well as in future publications.

The final report is to be submitted digitally in DAIM. An executive summary of the thesis including title, student's name, supervisor's name, year, department name, and NTNU's logo and name, shall be submitted to the department as a separate pdf file. Based on an agreement with the supervisor, the final report and other material and documents may be given to the supervisor in digital format.

Department of Energy and Process Engineering, 06.01. 2012

Olav Bolland
Department Manager

Torbjørn K. Nielsen
Academic Supervisor

Research Advisors:
Morten Kjeldsen, Flow Design Bureau AS

## Acknowledgements

This master thesis has been written at the NTNU Hydro Power Laboratory, in collaboration with Flow Design Bureau (FDB) in Stavanger.

I am most grateful to my supervisors Prof. Torbjørn Nielsen at NTNU and Dr. Morten Kjeldsen at FDB for their guidance and support during this semester.

I would also like to acknowledge M.Sc. Erlend Nøttveit for kindly sharing his experience with dynamic meshing in Fluent with me.

Finally, I have very much appreciated my year at the Hydro Power Laboratory and want to express my gratitude to all students and staff for creating a good academic and social environment.

_____

Anne Vea
Trondheim, 25.06.2012

**Summary**

A synthetic jet is a flow control device which injects a pulsating jet flow of high-momentum fluid into a boundary layer near the wall confining a main flow. The technique is used to prevent or delay boundary layer separation. While the method is well reported for gas flows, less knowledge is available for liquid flows. It has been suggested that synthetic jets might be used in hydro turbines in order to stabilise draft tube flow.

When accelerating a liquid flow, the energy consumption required will not only depend on the system mass, but also on the added mass due to acceleration of the liquid. The purpose of this thesis has been to study the physics of a synthetic jet where water is the working fluid, drawing special attention to added mass.

CFD simulations have been conducted, where the synthetic jet was modelled using a dynamic grid. Results for added mass and frequency response of the system from CFD analysis have been compared to an analytic solution. CFD simulations seem to have captured a number of interesting effects not predicted from the analytic solution; the most prominent being frequency regions of lower added mass than analytically predicted.

The apparent resonance regions are believed to occur due to interaction between the excitation frequency of the synthetic jet, and frequencies of dynamics in the system - examples are pressure pulsations from vortex shedding frequencies, or from frequencies originating from the effect of flow across a cavity.

Furthermore, it has been demonstrated that operating the system at resonance will reduce the power requirements of the driving force, and that a variable stiffness spring should be part of the actuation system to allow for tuning of the resonance frequency.

## Sammendrag

Innen strømningskontroll benyttes såkalte syntetiske jet'er til å hindre eller forsinke separasjon i en strømning. Metoden baserer seg på en pulserende jet som skytes inn i grensesjiktet til en hovedstrømning, slik at hovedstrømningens grensesjikt får tilført energi. Teknikken har vært mest brukt for gasstrømninger, spesielt innen luftfart. I væskestrømninger er bruken av syntetiske jet'er mindre kjent. Imidlertid er det foreslått at metoden kan egne seg til å stabilisere sugerørsstrømning i vannturbiner.

Kraften som trenges til å akselerere en væske er, ved siden av systemets masse, også avhengig av tilleggsmassen som oppstår på grunn av akselerasjonen. I denne oppgaven har en syntetisk jet blitt undersøkt spesielt med hensyn på tilleggsmasse av vannet.

Det er utført CFD-analyse av systemet, der den syntetiske jet'en er modellert ved hjelp av dynamiske mesh. Tilleggsmassen og frekvensresponsen til systemet er sammenliknet med en analytisk modell. CFD-resultatene viser noen interessante effekter som ikke kan sees fra den analytiske modellen. At tilleggsmassen er lavere enn forventet i enkelte frekvensområder er den mest fremtredende observasjonen.

Det er antatt at disse frekvensene er resonansfrekvenser som oppstår i samspillet mellom jet'ens eksitasjonsfrekvens og frekvenser av andre dynamiske fenomener, som virvelavløsning og frekvenser som oppstår ved strømning over en diskontinuerlig overflate.

I tillegg er det vist hvordan systemet kan drives i nærheten av resonansfrekvens for at minst mulig drivende kraft er nødvendig. En fjær med variabel fjærstivhet bør inngå i aktueringssystemet, slik at systemet kan manipuleres til å drives på resonans.

# Contents

# List of Figures

# List of Tables

# Nomenclature

| | | |
|---|---|---|
| $a$ | Acceleration | $\mathrm{m}/\mathrm{s}^2$ |
| $A$ | Area | $\mathrm{m}^2$ |
| $A_0$ | Amplitude | m |
| $A_{ref}$ | Reference area | $\mathrm{m}^2$ |
| $b_1, b_2$ | Coefficients in the Fourier Average Method | - |
| $c$ | Damping constant | $\mathrm{kg}/\mathrm{s}$ |
| $C^*$ | Amplification | N |
| $C_p$ | Pressure recovery coefficient | - |
| $d$ | Diameter of coil spring wire | m |
| $D$ | Diameter | m |
| $D$ | Diameter of coil spring | m |
| $D_0$ | Orifice diameter | m |
| $f$ | Frequency | Hz |
| $\vec{f}$ | Body forces | $\mathrm{kgm}^2/\mathrm{s}^2$ |
| $F$ | Force | N |
| $F_0$ | Force amplitude | N |
| $F_{avg}$ | Force averaged over one cycle | N |

| | | |
|---|---|---|
| $F_{ex}$ | Excitation force | N |
| $F_{friction}$ | Frictional force | N |
| $F_{nozzle}$ | Force from nozzle losses | N |
| $F_{shed}$ | Force from pressure fluctuations | N |
| $g$ | Gravity constant | $\text{m}/\text{s}^2$ |
| $G$ | Modulus of rigidity | Pa |
| $H$ | Piston height | m |
| $j$ | Counter variable | - |
| $k$ | Spring stiffness | $\text{N}/\text{m}$ |
| $k$ | Turbulent kinetic energy | $\text{kg}/\text{ms}^3$ |
| $k_1, k_2, k_j$ | Spring stiffness of spring 1, 2, j | $\text{N}/\text{m}$ |
| $k_{eq}$ | Equivalent spring stiffness | $\text{N}/\text{m}$ |
| $K_n$ | Nozzle loss coefficient | - |
| $K_{shed}$ | Shedding constant | - |
| $L$ | Stroke length ratio | - |
| $L_0$ | Stroke length | m |
| $m$ | Mass | kg |
| $m_{added}$ | Added mass | kg |
| $m_{added,an}$ | Analytic added mass | kg |
| $M$ | Total mass | kg |
| $n$ | Counter variable | - |
| $N$ | Normal force | N |
| $N$ | Number of coils in helical spring | - |
| $p$ | Pressure | Pa |

| | | |
|---|---|---|
| $p_1, p_2$ | Pressure at locations 1 and 2 in draft tube | Pa |
| $p_a$ | Atmospheric pressure | Pa |
| $p_{vap}$ | Vapour pressure of water | Pa |
| $Q$ | Flow rate | $kg/m^3$ |
| $Q_j$ | Volumetric discharge, synthetic jet | $m^3/s$ |
| $Q_m$ | Volumetric discharge, main flow | $m^3/s$ |
| $R$ | Radius | m |
| Re | Reynolds number | - |
| $\mathrm{Re}_{U_0}$ | Reynolds number, orifice | - |
| St | Strouhal number | - |
| $t$ | Time | s |
| $T$ | Length of time period | s |
| $u$ | Velocity in x-direction | $m/s$ |
| $\vec{u}$ | Velocity vector in x-direction | $m/s$ |
| $\bar{u_1}^2$ | Area-averaged velocity | $m/s$ |
| $U_\infty$ | Free-stream velocity | $m/s$ |
| $U_0$ | Time-averaged flow velocity through orifice | $m/s$ |
| $U_{RMS}$ | RMS value of velocity | $m/s$ |
| $v$ | Velocity in y-direction | $m/s$ |
| $\vec{v}$ | Velocity vector in y-direction | $m/s$ |
| $v_{avg}$ | Velocity averaged over one cycle | $m/s$ |
| $V_1, V_2$ | Velocity at locations 1 and 2 in draft tube | $m/s$ |
| $V_{piston}$ | Piston volume | $m^3$ |
| $w$ | Piston width | m |

| | | |
|---|---|---|
| x,y | Cartesian coordinates | m |
| $z_{losses}$ | Head loss | m |
| $\Delta h_0$ | Amplitude of piston stroke | m |
| $\Delta h(t)$ | Piston wall displacement at time $t$ | m |
| $\Delta p_{loss}$ | Pressure loss across nozzle | Pa |
| $\Delta t$ | Time step | s |
| $\epsilon$ | Turbulent dissipation | $\mathrm{m^2/s^3}$ |
| $\Gamma$ | Circulation | $\mathrm{1/ms^2}$ |
| $\mu$ | Dynamic viscosity | $\mathrm{Ns/m^2}$ |
| $\nu$ | Kinematic viscosity | $\mathrm{m^2/s}$ |
| $\nu$ | Friction coefficient | - |
| $\rho$ | Density | $\mathrm{kg/m^3}$ |
| $\rho_w$ | Density of water | $\mathrm{kg/m^3}$ |
| $\phi$ | Phase angle | rad |
| $\omega$ | Frequency | $\mathrm{s^{-1}}$ |
| $\omega$ | Specific dissipation rate | $\mathrm{1/s}$ |
| $\omega_n$ | Natural frequency | $\mathrm{s^{-1}}$ |

# Acronyms

**CFD**   Computational Fluid Dynamics

**DC**   Direct Current

**DNS**   Direct Numerical Simulation

**FDB**   Flow Design Bureau

**FEM**   Finite Element Analysis

**FSMA**   Ferromagnetic Shape Memory Alloy

**LES**   Large Eddy Simulation

**NiTi**   Nickel-Titanium

**NTNU**   Norwegian University of Science and Technology

**PZT**   Lead Zirconate Titanate

**RANS**   Reynolds-Averaged Navier-Stokes

**RMS**   Root Mean Square

**SMA**   Shape Memory Alloy

**SST**   Shear Stress Transport

**UDF**   User Defined Function

# Chapter 1

# Introduction

## 1.1   Background

Within the field of fluid dynamics, flow control focuses on how to reduce undesired effects in fluid flow systems. With knowledge of the underlying physical mechanisms, such as separation or transition from laminar to turbulent flow, measures can be taken to manipulate the flow. Normally, flow control is employed when a system does not operate at design conditions. Popular targets for flow control are drag reduction, lift augmentation or reduction of pressure fluctuations in a system. Although fluid dynamics forms the foundation for flow control, it can still be considered as an interdisciplinary field in the sense that other engineering fields are inevitably involved. Applied flow control solutions also include aspects of e.g. materials and control engineering.

Thanks to more than a century of flow control research, a wide range of techniques has been developed since Ludwig Prandtl did his pioneering work on boundary layer manipulation in 1904. One line of boundary layer flow control is represented by synthetic jets. These are used to delay boundary layer separation by injecting pulses of high-momentum fluid into boundary layers.

Up until now, synthetic jets have mainly been applied to gas flows, especially within the aerospace industry. Flow control techniques for hydro power

applications are of interest for the NTNU Hydro Power Laboratory. Co-advisor Dr. Morten Kjeldsen has suggested that the use of synthetic jets in water should be investigated with hydro turbine draft tube flow in mind. However, water as a working fluid introduces new challenges, the most prominent being issues related to added mass and cavitation.

## 1.2   Hypothesis

Synthetic jets are assumed to have a desirable influence on liquid flow. However, fluid instead of gas as the working medium poses a new challenge, in the sense that the effect of added mass can become significant in accelerating liquid flows. CFD simulations are assumed to give an indication of how added mass affects the operation of a synthetic jet in water.

## 1.3   Scope of work

The overall theme to be highlighted in this thesis is flow control techniques where adaptive geometries are involved. However, the questions as given in the problem descriptor sheet prior to this document are general, and can be approached in a number of ways. Thus, there was a need to narrow and more clearly define the objective of this work at an early stage.

Several interesting options related to control of vortex shedding and boundary layer separation were discussed. In agreement with advisors Prof. Torbjørn Nielsen and Dr. Morten Kjeldsen, dynamic modelling and CFD analysis of a water synthetic jet has been chosen as the main scopes of work. Additionally, attention will also be give to technologies to drive the synthetic jet system.

Synthetic jets were originally not among the options outlined in the project descriptor sheet which is enclosed on the first pages of this report. However, the topic is in line with the main intention given in the sheet; namely to study a system where added mass is relevant by means of CFD analysis with dynamic mesh.

## 1.4 Methodology

The numbered entries below refer to the question numbers as given in the sheet attached prior to this document.

**Question 1** will be approached by a literature study focusing on known techniques to delay boundary layer separation. Previous flow control works from the NTNU Hydro Power Laboratory will also be summarised. Next, simplified analytic models in both the time and frequency domain will be developed in order to obtain added mass and frequency response of a synthetic jet system, based on the physics of the problem under investigation.

**Question 2** includes all CFD work. A geometry model and mesh will be constructed, and CFD simulations will be run to investigate added mass effects. A parameter study of selected parameters will be conducted.

As there are no experimental results available for comparison, CFD results will be validated against results obtained from the analytic model developed in Chapter 3.

**Question 3** will take the form of a literature study on actuation systems for synthetic jets. Per se, the NTNU Hydro Power Laboratory does not have a laboratory rig for synthetic jet experiments. However, if flow control emerges as an area of research interest at the laboratory, a rig might be constructed in the future. Therefore, conventional actuators as well as system based on smart materials will be discussed, in order to highlight possible solutions for a future laboratory rig.

## 1.5 Limitations

This thesis aims at investigating synthetic water jets by means of analytic models and numerical simulations. The effects of added mass will be the main area of interest. Less emphasis will be placed on achieving detailed models of flow structures, interaction between the boundary layer and the synthetic jet, etc.

Furthermore, cavitation inevitably requires attention when using synthetic jets with water as the working fluid. Nevertheless, cavitation issues are out of scope of this work.

As the transient CFD analyses are run on a regular work station with only four cores available, the simulation domain has been restricted to 2D in order to obtain results within reasonable computational time. For the same reason, a RANS solver with a two-equation turbulent model was chosen rather than higher-order equation turbulence models or LES / DNS solvers.

## 1.6  Previous works on synthetic jets

Here, a short overview of works on synthetic jet will be presented. More flow control techniques are presented in Chapter 2.

Amitay and Glezer [2] studied the effect of using synthetic jets for reattachment of a separated shear layer on a stalled aerofoil. Laboratory experiments are conducted with the synthetic jet system located near the leading edge of the aerofoil. The method is considered as "fluidic modification" as it alters the apparent aerodynamic shape of the body due to displacement of streamlines. Particular emphasis was placed on the actuation frequency of the jet. While actuation frequency of the same order of magnitude as the vortex shedding frequency caused unsteady reattachment of the separated boundary layer, a frequency of ten times the vortex shedding frequency completely eliminated the vortex structures previously observed along the aerofoil surface. Additionally, Amitay and Glezer [2] demonstrated lift augmentation and drag reduction for a range of post-stall angles of attack when a synthetic jet was employed.

An experimental investigation of a synthetic jet with water as the working fluid can be found in Smith and Glezer [40]. Experiments were run for a round synthetic jet with orifice diameter 0.5 mm driven at resonance. Here, the authors demonstrated that the mean trajectory of the jet flow remains similar despite significant increase in the magnitude of the jet flow impulse. The article also includes a brief discussion on techniques to reduce the orifice diameter. Silicon micro-machining techniques are mentioned as one method to obtain small orifice diameters.

A CFD analysis of a synthetic jet is found in Ferlauto and Marsilio [15]. Although only one simulation of jet flow into quiescent air is described, a number of interesting aspects is presented. The authors argue that from a flow control perspective, the cavity region is of less interest than the region where the jet meets the external flow. Hence, grid resolution in a CFD model should

reflect this fact. In Ferlauto and Marsilio [15], the jet is generated by modelling the cavity as a piston with an oscillating boundary condition, so that $y(t) = A_0 \sin(\omega t)$.

Even if literature on synthetic jets in hydropower draft tubes has not been found, the application of synthetic jets in diffuser geometries has been studied. The experimental study of Nishi et al. [32] assessed the effect of a so-called vortex generator jet on boundary layer separation in a conical diffuser geometry, using air as the working medium. The pressure recovery coefficient ($C_p$; Equation. 2.11) is observed to improve for velocity ratios of 1 and higher, and increases with higher velocity ratios. Here, the velocity ratio is defined as the ratio of jet velocity to main flow velocity. More moderate increases in $C_p$ are observed when increasing the ratio of jet discharge to main flow; $Q_j/Q_m$. Nishi et al. [32] suggested that the velocity ratio between jet flow and main flow therefore should be chosen as a design parameter.

## 1.7 State of the art of synthetic jets for flow control

A number of articles from the last decade leaves no doubt that jets with harmonic fluid input, rather than steady injection, will dominate the future efforts to control boundary layer separation. One major advantage of the synthetic jet technology is its compact and relatively simple construction, where the device is "hidden" from the flow.

Zhang et al. [49] argued that within the aerospace industry, a transition from conventional passive flow control devices (flaps and spoilers) to modern active flow control technology is emerging. Next, they claim the joint efforts of Air Force Research Laboratory, Lockheed Martin Aeronautics Company and General Electric, which resulted in a successful full-scale test of the synthetic jet using the F-16 fighter aircraft, to be a milestone in that respect. Synthetic jets have also proved to delay stall and increase the lift-to-drag ratio for aerofoils. Hence, synthetic jets for aerospace applications appear as the most feasible area of application. Zhang et al. [49] proposed that in the future, synthetic jets might also be used for separation control in turbo fans.

Research on synthetic jets appears to have been of more interest for air force aerospace applications than for civil passenger or transport aircrafts. One

laboratory case study is found in Gomes and Crowther [19]. Here, synthetic jets for application in an Airbus A321 commercial aircraft is discussed, for both low and high speed (take off/landing and cruising, respectively). However, Gomes and Crowther's [19] work dates back to 2008. For Airbus' most recent passenger aircraft A380, no articles reporting on topics related to synthetic jets are found.

Precise and small-size, low weight actuation system are now commercially available, based on recent developments in piezoelectric materials and shape memory alloy (SMA) composites. The development of efficient and high-quality actuation systems are of great importance for the synthetic jet technology as a whole.

The future of the synthetic jet technology seems bright. However, Zhang et al. [49] highlighted the fact that despite efforts to arrive at an optimal synthetic jet design (particularly with respect to geometry), no conclusive results have yet been obtained.

# Chapter 2

# Theory

## 2.1 Fluid dynamics

### 2.1.1 Governing equations

The CFD solver used in this project is a Reynolds-Averaging Navier-Stokes (RANS) solver, which solves a discretised formulation of the Navier-Stokes equations. For a Newtonian, incompressible fluid, the compact form of the Navier-Stokes equations can be found in White [47] in compact form as

$$\rho\left(\frac{\partial \vec{v}}{\partial t} + \vec{v} \cdot \nabla \vec{v}\right) = -\nabla p + \mu \nabla^2 \vec{v} + \vec{f} \tag{2.1}$$

In 2D, Equation 2.1 can be rewritten explicitly in x-direction:

$$\rho\left(\frac{\partial u}{\partial t} + u\frac{\partial u}{\partial x} + \frac{\partial u}{\partial y}\right) = -\frac{\partial p}{\partial x} + \mu\left(\frac{\partial^2 u}{\partial x^2} + \frac{\partial^2 u}{\partial y^2}\right) + \rho g_x \tag{2.2}$$

and in y-direction:

$$\rho\left(\frac{\partial v}{\partial t} + v\frac{\partial v}{\partial x} + \frac{\partial v}{\partial y}\right) = -\frac{\partial p}{\partial y} + \mu\left(\frac{\partial^2 v}{\partial x^2} + \frac{\partial^2 v}{\partial y^2}\right) + \rho g_y \tag{2.3}$$

Refer to Appendix A for details on Reynolds averaging and turbulence modelling.

### 2.1.2  Boundary layers

A boundary layer is the fluid region between a free-stream and a solid wall. The commonly accepted definition of the boundary layer thickness is the height $y$ at which the velocity in the boundary layer $u(y)$ equals 99 % of the free-stream velocity $U_\infty$. At the wall, the no-slip condition dictates zero velocity. Different boundary layer velocity profiles are displayed in Figure 2.1.



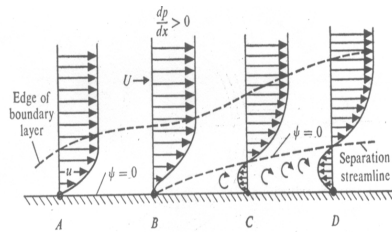**Figure 2.1:** Profiles A to D are possible velocity profiles in a boundary layer. Figure from [9]

Velocity profiles C and D in Figure 2.1 depict a situation of an adverse pressure gradient and hence boundary layer separation.

### 2.1.3  Non-dimensional quantities in fluid dynamics

The ratio of inertial to viscous forces is a function of the non-dimensional Reynolds number:

$$\mathrm{Re} = \frac{\rho U D}{\mu} \tag{2.4}$$

Flow regimes can be characterised by the value of Reynolds number. Sumer and Fredsøe [41] have described flow around a bluff body, namely a circular cylinder, for various Reynolds number flow regimes. For Reynolds numbers below 5, no vortices are present downstream of the body. In the Reynolds number range from 5 to 40, a vortex pair can be observed in the wake region. For Reynolds number of 40 and higher, the formation of a von Karman vortex street is found. Here, pairs of counter-rotating vortices are shed downstream of the body. The vortex shedding frequency is given by the non-dimensional Strouhal number:

$$\mathrm{St} = \frac{fD}{U} \tag{2.5}$$

Besides predicting vortex shedding frequency, the Strouhal number is also commonly used to obtain a non-dimensional frequency.

At around $\mathrm{Re} > 200$, the flow behind a cylinder undergoes transition to a turbulent wake. In the sub-critical Reynolds number regime from $\mathrm{Re} = 300$ to $\mathrm{Re} = 3 \times 10^5$, the wake is turbulent while the boundary layer is laminar. A further increase in Reynolds number leads to a transition from laminar to turbulent boundary layer separation.

### 2.1.4 Pressure fluctuations in flow across a cavity

For fluid flow in pipes or across surfaces where a cavity is present, pressure and velocity fluctuations may occur due to the geometric discontinuity experienced by the flow. Kuo and Jeng [25] explained the mechanism behind the development of these oscillations in the following steps

1. Flow separates at the upstream lip of the cavity, leading to the formation of an unstable shear layer.

2. The unstable shear layer hits the downstream cavity lip, and the resulting pressure fluctuation is reflected back to upstream lip. Hence, self-sustaining pressure fluctuations can develop at the natural frequency of the instability.

Additionally, Kuo and Jeng [25] found that the following parameters to influence the pressure fluctuations:

- Free-stream velocity $U_\infty$

- Momentum thickness of upstream boundary layer

- Cavity geometry

This list of influencing parameters has been established by experiments rather than through theoretic analysis.

While research results for air and other gas flows have been thoroughly reported, less knowledge is available for liquid flows. Lee et al. [26] summarised the results from a number of hydrodynamic studies on flow past cavities, giving most emphasis to articles which suggest that similar pressure fluctuations are evident in water flows as well as in gas flows, though weaker. Nevertheless, articles where no fluctuations are reported are also mentioned. Lee et al. [26] also conducted DNS and LES for water at various Reynolds number, and observed self-sustaining pressure fluctuations.

Experiments in a flow tunnel were performed by Kuo and Jeng [25]. Here, a rotating cylinder at a given excitation frequency was observed to cause a lock-in phenomenon in the sense that the frequency of the instabilities was locked to the excitation frequency over a range of Reynolds number.

## 2.1.5   Added mass

The term "added mass" refers to the additional force required to accelerate a solid body through a fluid. As the body and the fluid cannot occupy the same volume simultaneously, a force is required to displace the fluid. This force is normally neglected in gas flows. For liquid flows, the force can be significant due to the high density of liquids relative to gases. By definition, the added mass force is in phase with the acceleration. This force can be expressed in terms of a mass so that Newton's 2nd law yields

$$F = (m + m_{added}) \cdot a \qquad (2.6)$$

Added mass depends on the body's modes of motion - transversal or rotational along or around the x-, y- and z-axis, and will also depend on the frequency of time-periodic motion. Added mass in direction $i$ due to motion in direction $j$ can be expressed in a matrix of dimension 6x6:

$$m_{i,j} = \begin{pmatrix} m_{1,1} & m_{1,2} & \cdots & m_{1,6} \\ m_{2,1} & m_{2,2} & \cdots & m_{2,6} \\ \vdots & \vdots & \ddots & \vdots \\ m_{6,1} & m_{6,2} & \cdots & m_{6,6} \end{pmatrix}$$

A more elaborate derivation of added mass for the synthetic jet system under investigation in thesis has been left to Section 3.2.

## 2.2 Introduction to flow control

### 2.2.1 Definition

Flow control is by co-advisor Morten Kjeldsen defined as "The collection of techniques that improve off-design performance or reduce deleterious effects in fluid flow systems, with a minimum of influence on the system where the technique is deployed."

### 2.2.2 Classification

Flow control is most commonly classified with respect to the power required for the control method. Passive flow control requires no power or control loop, whereas power input is required for active flow control. Furthermore, active control comprises both the predetermined methods with no loop and the reactive methods where a control loop is involved. As a synthetic jet requires a periodic excitation force, the system belongs to the active flow control category.

Hak [21] has given a broad and comprehensive introduction to several aspects of flow control. He identified the most important targets for flow control as:

- Drag reduction

- Lift enhancement

- Mixing augmentation

- Noise suppression

### 2.2.3   Techniques and applications

Hak [21] has explained how the purpose of flow control varies with the Reynolds number regime. For Reynolds numbers below $1 \times 10^6$, Hak suggested to emphasize laminar shear stress reduction. This corresponds fairly well to the definition in White [47], which says that transition to turbulent flow normally occurs at Reynolds numbers of $5 \times 10^5$ and higher, but that delay of transition still is possible for Reynolds numbers beyond this. In the flow regime where Reynolds numbers range from $1 \times 10^6$ to $4 \times 10^7$, Hak suggested flow control to delay transition using stability modifiers, e.g. flexible walls, which are described in the following section. Beyond Reynolds numbers of $4 \times 10^7$, there are no known methods to prevent transition.

Hak [21] discussed several flow control methods involving adaptive geometries. One entire chapter is devoted to the topic of passive compliant coatings; flexible walls which, depending on the physical properties of the coating, can be used to delay or promote transition or separation. The first experiments on flexible coatings were conducted in the late 1950's, motivated by the favourable properties of the dolphin's skin.

The purpose of a compliant coating is to modify the velocity profile of the flow by generating waves. Compliant coatings are observed to be most efficient when the generated waves are of the same frequency and phase speed, but of opposite phase. In this case, experiments have proved that transition due to the instabilities in the boundary layer can be eliminated. Hak [21] argues that the density of the coating material should be close to that of the surrounding fluid. Hence, this technique is feasible for hydrodynamic applications only.

A number of geometry modification techniques used to suppress vortex shedding has been reviewed by Zdravkovich [48]. In his article of 1980, Zdravkovich gave a broad and comprehensive introduction to methods developed between the 1950's and 1978. The techniques are classified in three categories:

- Surface protrusions
- Shrouds
- Nearwake stabilisers

Within each category, Zdravkovich [48] also distinguished between unidirectional and omnidirectional means. Unidirectional methods require one specific velocity

direction, whereas omnidirectional methods do not impose constraints on flow direction.

## 2.3   Synthetic jets

In the following, the synthetic jet technology is the flow control method that will be given most attention. Synthetic jets are primarily used to delay separation or stabilise separation points. Figure 2.2 displays a schematic of the synthetic jet system. This device is attached beneath the wall confining the main flow - e.g. an beneath the surface of an aerofoil or draft tube.
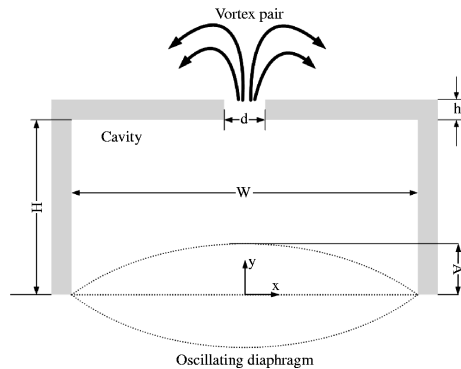


**Figure 2.2:** Schematic of syntehtic jet with cavity and orifice beneath a free stream. Here, the jet flow is driven by an oscillating and deforming diaphragm. Figure from [36]

In a synthetic jet, the working fluid is the same as in the cross-flow. The working principle of the jet is based on a two-stroke principle, where fluid flow through the orifice is driven by the motion of a piston or diaphragm. During the suction stroke, fluid is drawn from the cross-flow into the cavity. The following blowing stroke ejects the entrained fluid through an orifice and back into the cross flow. This two-stroke cycle introduces no net mass addition or subtraction to the system.

The jet flow causes formation of vortex rings propagating from the orifice into the cross-flow. Their speed of propagation is critical; insufficient velocity will cause the vortex structured to be drawn back into the cavity during suction

stroke. Biot-Savart's law, as given in Anderson [3], can be applied to find the self-induced velocity of vortex rings.

$$\vec{u} = \frac{\Gamma}{4\pi} \int \frac{d\vec{s} \times \vec{r}}{|\vec{r}|^3} \qquad (2.7)$$

Hence, the self-induced velocity at a given point P along the z-axis is

$$\vec{u} = \frac{\Gamma R^2}{2(R^2 + z^2)^{3/2}} \vec{k} \qquad (2.8)$$

Zhang et al. [49] specified the parameters which influences the formation of vortex rings as

- dimensions of cavity and orifice

- density and viscosity of working fluid

- amplitude of diaphragm movement

- oscillation frequency of diaphragm

Based on the above parameters, a stroke length ratio and a Reynolds number are defined. The stroke length ratio $L$ represents the length of the jet column $L_0$ to the diameter of the orifice $D_0$. The velocity factor of the Reynolds number is the average jet velocity during blowing stroke, while the length factor is the orifice diameter.

$$L = \frac{L_0}{D_0} \qquad (2.9)$$

$$\mathrm{Re}_{\mathrm{U_0}} = \frac{U_0 D_0}{\nu} \qquad (2.10)$$

$U_0$ represents the flow velocity out of the orifice, time-averaged over one blowing stroke of time period $T$. Hence, the stroke length $L_0 = U_0 T$. Circulation increases with stroke length. According to Zhang et al. [49], for stroke length ratios $L > 4$, a secondary vortex is shed behind the primary vortex rings. Similar findings ($L > 4 - 5$) are reported in more papers, e.g in Akhmetov [1].

Zhang et al. [49] explained that, given sufficient vortex ring velocity, the vortex rings will energize the boundary layer by momentum transfer. The region closest to the wall in a boundary layer is associated with low-speed fluid flow, compared to the outer part of the layer. As the high-speed jet is injected into the low-speed region of the boundary layer, low-speed fluid is lifted up. Hence, the adverse pressure gradient which causes separation can be prevented.

## 2.4   Flow control in hydro power draft tubes

In a hydropower plant, the draft tube is the conduit in which water is transported from the runner exit to the lower reservoir. Its purpose is to recover kinetic energy to pressure energy. The performance can be calculated in terms of the pressure recovery factor $C_p$. The following definition of $C_p$ is given in Nishi et al. [32]:

$$C_p = \frac{p_a - p_1}{\rho \bar{u}_1{}^2} \tag{2.11}$$

The nominator of Equation 2.11 decribes static pressure rise, whereas $\bar{u}_1$ in the denominator is an area-averaged velocity, i.e. $Q/A_{ref}$.

According to Equation 2.12 (Bernoulli's equation), a pressure increase can be achieved by retarding the flow.

$$z_1 + \frac{p_1}{\rho g} + \frac{V_1{}^2}{2g} = z_2 + \frac{p_2}{\rho g} + \frac{V_2{}^2}{2g} + z_{losses} \tag{2.12}$$

As described by Wei et al. [46], the regular draft tube design provides deceleration by an increase in draft tube cross-sectional area. The normal shape of a the upper section of a draft tube for a Francis turbine is the frustum of a cone. It is desirable to maintain attached flow along the walls of the draft tube. Hence, the cone angle must be limited due to avoid the possibility of flow separation. Rules of thumb indicate an angle of $3 - 3.5°$ degrees between cone centreline and wall. Future successful application of synthetic jets can lead to more compact draft tube designs. If a more rapid expansion of cross-sectional area is possible without separation, a shorter draft tube length is required to decelerate the flow.

## 2.5  Flow control studies at the NTNU Hydro Power Laboratory

Flow control has been investigated in a number of works at the NTNU Hydro Power Laboratory in Trondheim. In his doctoral thesis, Francke [17] investigated how pressure pulsations related to swirling flow in hydro turbine draft tubes could be attenuated using water injection. A water injection system, consisting of nozzles around the circumference of a draft tube, was developed and tested. As for a synthetic jet system, the objective was to prevent instabilities in draft tube flow. Francke's [17] system system differs from a synthetic jet in the sense that water injection is steady rather than pulsation, and that the injected water is a bypass flow which is led past the turbine.

Vekve [43] did also study swirling draft tube flow experimentally. His work focused on how cone geometry influenced pressure oscillations in the draft tube. Vekve found that for several of the investigated cone geometries, fluctuations could be significantly reduced and that for one particular geometry, the flow field exhibited no sign of the vortex core instability at all. Hence, cone modification can serve as a technique to employ passive flow control downstream of a Francis turbine.

Motivated by the tubercles found on humpback whale flippers, Vilberg [44] investigated hydrofoils with and without leading edge tubercles in order to determine the influence of tubercles on lift and drag. Her project thesis include 2D and 3D CFD simulations for static and oscillating hydrofoils. For static hydrofoils, the exact location of the separation point has not been determined due to discrepancies between different codes and turbulence models used. However, after clearly reaching the post-stall flow regime, a distinct difference was found for drag coefficient with and without leading edge tubercles. Simulations of oscillating hydrofoils proved to be highly dependent on oscillation frequency and no conclusive results were obtained.

In his recent master thesis, NTNU graduate Ekanger [13] discussed whether morphing flow control concepts used for aeroplanes are applicable for hydropower purposes. Rotor-stator interaction in Francis turbines is mentioned as one possible situation where morphing can be used for flow control. The concept of varying the camber of turbine guide vanes is explored by means of a CFD code. Morphing was assumed to enhance turbine efficiency when operating at part load.

In addition to his CFD work, Ekanger [13] also designed and conducted a laboratory experiment of flow at Re $= 2000 - 5000$ around a cylinder with and without semi-spherical surface rubber bumps. Measurements revealed that, given a sufficient diameter of the bumps, the vorticity amplitude was reduced when compared to the results from flow around a regular cylinder. Based on his results, Ekanger [13] concluded that the surface bumps can be used for flow control purposes.

# Chapter 3

# Theoretical model for synthetic jet

In this chapter, a simple analytical model for a synthetic jet as shown in Figure 3.1 will be developed based on the physics of the problem. First, a theoretical model for force and power will be presented. Next, a method to calculate added mass will be outlined. Finally, a dynamic model in the frequency plane will be developed.
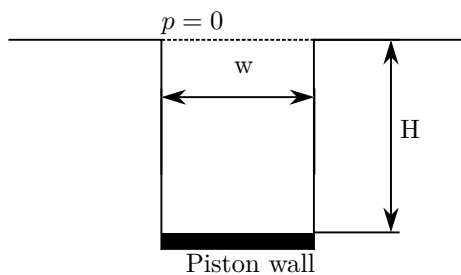


**Figure 3.1:** Analytic model, added mass

## 3.1 Analysis of the synthetic jet as a mechanical mass-spring system

The time-varying motion of the piston can be expressed as

$$\Delta h(t) = \Delta h_0 \sin(\omega t) \tag{3.1}$$

where

$$\omega = 2\pi f \tag{3.2}$$

Consequently, velocity can be expressed as

$$\frac{d\Delta h(t)}{dt} = \Delta h_0 \omega \cos(\omega t) \tag{3.3}$$

and acceleration as

$$\frac{d^2 \Delta h(t)}{dt^2} = -\Delta h_0 \omega^2 \sin(\omega t) \tag{3.4}$$

Applying a force so that the piston moves horizontally will accelerate the mass of water. Newton's 2nd law of motion $F = ma$ gives

$$\overbrace{p(t) \cdot A}^{F} = \overbrace{\rho_{water} h_0 A}^{m} \overbrace{\frac{d^2(\Delta h(t))}{dt^2}}^{a} \tag{3.5}$$

As the area cancels out on both sides of the equality, the pressure can be written as

$$p(t) = \rho_{water} h_0 \frac{d^2(\Delta h(t))}{dt^2} \tag{3.6}$$

A major concern should be whether cavitation can occur during the suction stroke of the synthetic jet. This possible presence of cavitation imposes the constraint $p(t) > p_{vap}$ for all $t$.

The average power required to accelerate the mass of water throughout one cycle of piston motion is the product of the time-averaged force and fluid velocity

$$P = F_{avg} \cdot v_{avg} = \frac{1}{T} \int_{t=0}^{t=T} p(t) A \frac{d(\Delta h(t))}{dt} dt \qquad (3.7)$$

Substituting $\Delta h(t)$ from Equation 3.1 and $p(t)$ from equation 3.6 into Equation 3.7 reveals that power is a function of $f^3$.

A mass-spring system can model the excitation force on the piston:

$$F_{ex}(t) = \sum M \cdot \frac{d^2(\Delta h(t))}{dt^2} + c \cdot \frac{d(\Delta h(t))}{dt} + k \cdot \Delta h(t) \qquad (3.8)$$

As $\sum M = m_{piston} + m_{added}$, this well-known second order ordinary differential equation takes both piston mass and added mass due to acceleration of fluid into account.

In order to obtain the oscillating motion of the piston, $F_{ex}$ is a time-varying driving force of the form $F_{ex} = F_0 \cos(\omega t)$.

The amplification factor $C^*/F_0$ depends on $\omega$, and typically yield a graph which peaks at the resonant frequency of the system;

$$\omega_n = \sqrt{\frac{k}{\sum M}} = \sqrt{\frac{k}{m_{piston} + m_{added}}} \qquad (3.9)$$

Starting from a homogeneous linear ODE, a complete derivation of the amplification factor $C^*/F_0$ is given in Kreyszig [24].

In order to use a minimum of energy to drive the system, it is desirable to operate the system at its resonance frequency, i.e. so that the frequency of the exciting force and the eigenfrequency of the system coincide: $\omega = n \cdot \omega_n$. As the system mass is fixed, altering the spring stiffness is the only way to control $\omega_n$. Possible practical configurations for varying spring stiffness will be discussed later.

## 3.2    Added mass

### 3.2.1    Analytic solution for synthetic jet

Here, an analytic estimate for added mass is simply the mass of water in the piston, $\rho V_{piston}$. For a 2D case,

$$m_{added,an} = \rho_w w H \tag{3.10}$$

is valid for a geometry similar to the synthetic jet depicted in Figure 3.1.

From Equation 3.10, it becomes clear that the analytic added mass solely depends on piston geometry since water is treated as an incompressible fluid.

### 3.2.2    Added mass computed from force

The magnitude of the added mass force is of interest. Aronsen [6] presented the Fourier-average method as a way to calculate the force in phase with acceleration. The Fourier-average method will be used in the present study to estimate added mass for the operation of a synthetic jet.  The following derivation of the method is given in Aronsen [6].

In the Fourier-average method, excitation force on the piston is assumed to be of the form

$$F(t) = F_0 \sin(\omega t + \phi) \tag{3.11}$$

when the motion of the piston can be described with the function

$$\Delta h(t) = \Delta h_0 \sin(\omega t) \tag{3.12}$$

$\phi$ is the phase angle between the two signals.

Next, $F(t)$ is assumed equal to a linear combination of an acceleration component and a velocity component:

$$b_1 \cdot \frac{d\Delta(h(t))}{dt} + b_2 \cdot \frac{d^2(\Delta h(t))}{dt^2} = F_0 \sin(\omega t + \phi) \tag{3.13}$$

Coefficients $b_1$ and $b_2$ can be found using the method of least squares, while $d\Delta h(t)/dt$ and $d^2\Delta h(t)/dt^2$ are given in Equations 3.3 and 3.4.

It is possible to expand the right hand side of Equation 3.13 using trigonometric identities:

$$F_0 \sin(\omega t + \phi) = F_0 \sin(\phi) \cos(\omega t) + F_0 \cos(\phi) \sin(\omega t) \tag{3.14}$$

Finally, Equation 3.13 can be rewritten in full length as

$$
\begin{aligned}
b_1 \Delta h_0 \cos(\omega t) - b_2 \Delta h_0 \omega^2 \sin(\omega t) \\
= F_0 \sin(\omega t + \phi) \\
= F_0 \sin(\phi) \cos(\omega t) + F_0 \cos(\phi) \sin(\omega t)
\end{aligned}
\tag{3.15}
$$

Considering the components of Equation 3.15, the equation can be split into a system of two equations

$$F_0 \sin(\phi) = b_1 \cdot \omega \Delta h_0 \tag{3.16}$$

$$F_0 \cos(\phi) = -b_2 \cdot \omega^2 \Delta h_0 \tag{3.17}$$

Equations 3.16 and 3.17 are implemented in a Matlab script in order to finally obtain $F_0$ for the system at every $\omega$ and $\Delta$. $F_0$ is the amplitude of the force in phase with acceleration. The amplitude of acceleration; $\Delta h_0 \omega^2$, is obtained from Equation 3.4. Hence, added mass is defined as

$$m_{added} = \frac{F_0}{\Delta h_0 \omega^2} \tag{3.18}$$

i.e. the ratio between the added mass force amplitude and the acceleration amplitude.

## 3.3    Dynamic model in the frequency domain

In dynamic systems, the frequency response is a measure of the magnitude of force applied to the system when altering the frequency of the system. The frequency response analysis is performed in the *s*-domain, where $s = j\omega$.

As far as possible, the dynamic model should reflect effects which are expected to occur in a real synthetic jet system. Therefore, nozzle losses and effects related to unsteady pressure across the orifice are also included in the model.

Nozzle losses are present when the flow experiences a contraction with a subsequent expansion on its way through the orifice between the cavity and the main flow region. Nozzle losses for various geometry configurations and diameter ratios are tabulated in Idelchik and Steinberg [22]. For the synthetic jet nozzle with dimensions as given in section 4.2, $K_n = 2.27$, where $K_n$ is defined as

$$K_n = \frac{\Delta p_{loss}}{\frac{1}{2}\rho v \cdot |v|} \tag{3.19}$$

Since nozzle loss in terms of force is $\Delta p_{loss} A$, the force related to nozzle losses can be expressed as

$$F_{nozzle} = K_n \cdot \frac{1}{2}\rho v \cdot |v| A \tag{3.20}$$

It is also assumed that an unsteady pressure field will develop across the nozzle exit due to the vortex shedding downstream of the orifice. This effect will cause a time-varying force which is denoted $F_{shed}$. Prior to the simulations, no information exists on the magnitude and frequency of $F_{shed}$. Here, it has been assumed that the pressure fluctuations can be described as a sine function where the frequency is equal to the frequency of the excitation force,

$$F_{shed} = K_{shed} \sin(\omega t) \tag{3.21}$$

From Equation 3.1, it becomes clear that $F_{shed}(t)$ is of the same form as $x(t)$. Therefore, it has been chosen to represent $F_{shed}(t)$ as an additional spring force, i.e. $F_{shed}(t) = K_{shed}x(t)$.

Other pressure fluctuations of frequencies different from the excitation frequency may also be present in the system, one example being the self-sustaining pressure

oscillations across the cavity as described in Section 2.1.4. However, the possible effect of such disturbances has in the following not been included because no knowledge exist on neither their magnitude nor their frequency.

The force balance

$$\sum F = ma = m\ddot{x} \tag{3.22}$$

can for the synthetic jet be rewritten as

$$m\ddot{x} + m_{added}\ddot{x} + c\dot{x} + K_n \cdot \frac{1}{2}\rho A\dot{x} \cdot |\dot{x}| + (K_{shed} + k)x = F_{ex} \tag{3.23}$$

The Laplace transform of Equation 3.23 is used for frequency analysis. However, the term $K_n \cdot \frac{1}{2}\rho A\dot{x} \cdot |\dot{x}|$ is non-linear and cannot easily be transformed. A linear approximation to Equation 3.23 can be obtained by linearising $\dot{x}|\dot{x}|$ around a point of operation $\dot{x}^P$ and replacing $x, \dot{x}, \ddot{x}$ with $x_1, x_2 = \dot{x_1}, \dot{x_2}$, respectively.

Equation 3.23 can be rewritten to obtain an expression for $\dot{x_2}$:

$$\dot{x_2} = \frac{1}{m + m_{added}}(F_{ex} - x_2 c - K_n \cdot \frac{1}{2}\rho A x_2 |x_2| - (K_{shed} + k)x_1) \tag{3.24}$$

Several methods exist for linearising non-linear terms. Balchen et al. [7] suggested to represent the linearised version of Equation 3.23 by the system

$$\Delta\dot{\mathbf{x}} = A\Delta\mathbf{x} + B\Delta\mathbf{u} \tag{3.25}$$

where the general form of the matrix A is given as

$$A = \begin{bmatrix} \frac{\partial f_1}{\partial x_1} & \frac{\partial f_1}{\partial x_2} \\ \frac{\partial f_2}{\partial x_1} & \frac{\partial f_2}{\partial x_2} \end{bmatrix}$$

and

$$\begin{aligned} \dot{x_1} &= f_1 \\ \dot{x_2} &= f_2 \end{aligned} \tag{3.26}$$

Another option is given by Faltinsen [14]. He introduced the substitution of the term $|x_2^P|$ with $|u_{RMS}|$. For the following work, Faltinsen's method has been chosen. Now, the linearised approximation of Equation 3.23 is ready to be transformed into the frequency domain.

An equivalent representation of the linearised version of Equation 3.23 in the frequency domain is given as a block diagram in Figure 3.2 where the $^1/_s$ blocks represent integration.
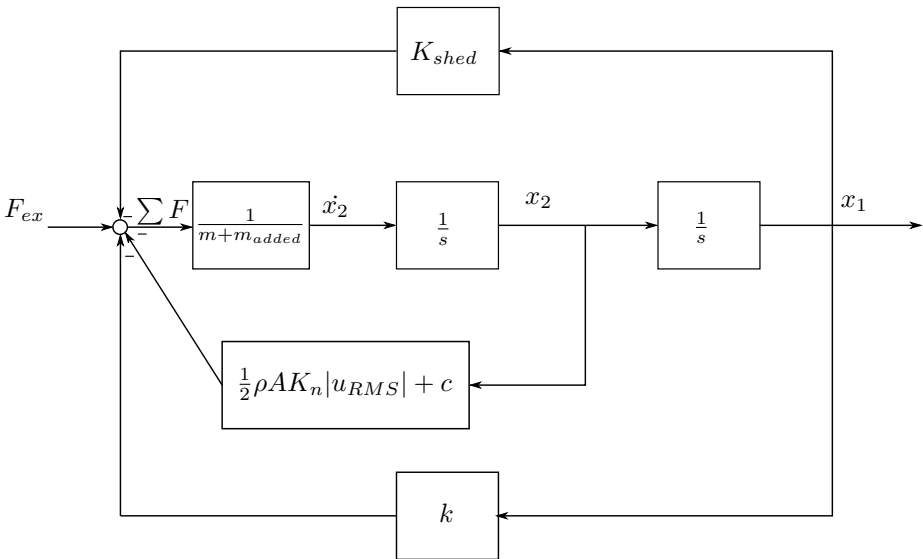


**Figure 3.2:** Dynamic model of synthetic jet system

By moving the take-off points towards the $x_1$ side, collapsing the parallel paths and finally eliminating the feedback loop, the system is reduced to an equivalent representation of the form $F(s) \cdot H(s) = X(s)$, as shown in Figure 3.3 and Equation 3.27
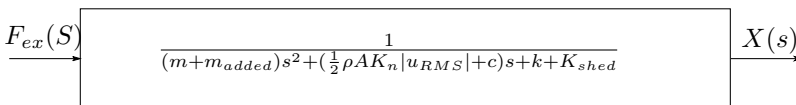


**Figure 3.3:** Reduced block diagram - equivalent to Figure 3.2

$$H(s) = \frac{1}{(m + m_{added})s^2 + (\frac{1}{2}\rho AK_n|u_{RMS}| + c)s + k + K_{shed}} \tag{3.27}$$

$H(s)$ represents the system's transfer function from excitation force input to displacement output. Substituting $s$ with $j\omega$ takes us from the Laplace domain to the complex Fourier domain, from which we can obtain the frequency response of the system.

$$H(j\omega) = \frac{1}{-(m + m_{added})\omega^2 + (\frac{1}{2}\rho AK_n|u_{RMS}| + c)j\omega + k + K_{shed}} \tag{3.28}$$

It is interesting to find the magnitude of the transfer function; $|H(j\omega)|$. Transfer functions with constant coefficients are commonly plotted as against $\omega$ as curves in Bode diagrams. Although the transfer function as given in Equation 3.27 now is linear, both $m_{added}$ and $|u_{RMS}|$ are assumed to be frequency dependent. Thus, it is necessary to calculate $m_{added}$ and $|u_{RMS}|$ first before finding $|H(j\omega)|$ at that particular frequency.

The root-mean-square (RMS) of a sine function $A\sin(\omega t)$ is $A/\sqrt{2}$. Since the velocity follows a sine (or cosine) function, $|u_{RMS}|$ has been defined as

$$u_{RMS} = \frac{\Delta h\omega}{\sqrt{2}} \tag{3.29}$$

From Equation 3.18, it becomes clear that $m_{added}$, which appears twice in the denominator of Equation 3.28, is also frequency dependent.

Equation 3.28 was implemented in a Matlab script which read the results from the CFD simulations so that the variables $\omega$, $m_{added}$ and $|u_{RMS}|$ were computed for each case. Then, the built-in Matlab commands `tf` and `evalfr` were used to calculate the frequency response corresponding to each CFD case. With this formulation of the transfer function, it is desirable to obtain high values of $|H(j\omega)|$, i.e. maximum displacement with a minimum of excitation force.

Parameters $\omega$ and $m_{added}$ are input and output from CFD simulations, $K_n$ is determined by means of tabulated values, while $m$, $c$, $k$ and $K_{shed}$ need to be estimated. From Equation 3.28, it is apparent that the force related to $K_{shed}$ can be seen as an additional spring force, and hence a contribution to

**Table 3.1:** Estimated parameters

| | |
|---|---|
| $m$ | negligible |
| $c$ | $10\,\mathrm{kg/s}$ |
| $k$ | $10\,\mathrm{N/m}$ |
| $K_{shed}$ | $0.1k = 1\,\mathrm{N/m}$ |

overall stiffness. Here, it has been assumed that $K_{shed} = 0.10k$. A summary of parameters are listed in Table 3.1.

# Chapter 4

# Numerical simulations of synthetic jet

## 4.1 Software

All work related to CFD simulations has been carried out within the ANSYS 13.0 software environment. The geometry was constructed using Ansys Design Modeler. For meshing, ANSYS Meshing was used. ANSYS Fluent has been used to solve all CFD cases. Fluent was also used for graphical post-processing, while the remaining post-processing was done with MATLAB.

## 4.2 Geometry

Synthetic jets might become a field of research interest at the NTNU Hydro Power Laboratory in the years to come. Despite the fact that no laboratory facilities for a synthetic jet rig are planned, dimensions of the CFD model are set to correspond with a possible future laboratory set-up. Hence, the dimensions should be sufficiently large for e.g. traversing a pitot tube.

The most common shape of a synthetic jet configuration seems to be a cavity with a contraction near the main cross-flow. Thus, the latter shape has been

chosen for CFD simulations in this project, with a ratio of cavity diameter to
orifice diameter of 5. Reports on rectangular, high aspect-ratio synthetic jets,
where cavity and orifice diameters are equal, have also been found, though less
frequently. An example of a 2D rectangular geometry referred to in this project
is the 0.5 mm wide, 75 mm high cavity found in Smith and Glezer [40].

Although most articles present experiments with significantly smaller orifice
diameters, the orifice diameter of this model will be 2 mm in order to avoid
complex and expensive manufacture. This diameter is believed to be practicably
realisable at the NTNU Hydro Power Laboratory, without exceeding dimensions
reported in literature. Among synthetic jets with orifice diameters in the order
of $10^{-3}$ m are the two jets of Mane et al. [30] with orifice diameters 2 mm and
3.67 mm, on which experiments and CFD simulations have been conducted. The
orifice geometry has been constructed with straight vertical walls for simplicity.

There seems to be no general guidelines for optimal cavity height. While Smith
and Glezer [40] and Mane et al. [30] designed cavities of heights 75 mm and
89 mm, respectively, other cavities are only a few millimetres high. In this
study, the cavity height is 40 mm.

A surface protrusion with excessive curvature has been included in the system
to promote boundary layer separation. Its shape is semicircular, with diameter
20 mm.

## 4.3   Dynamic grid

Simulations in which the geometry is changing, require the use of dynamic grids.
Dynamic grids differ from regular time-constant grids in the sense that cells may
change shape, disappear or merge during a transient simulation. In this case,
the piston is the only moving domain. Hence, the grid has been divided into
zones, so that all cells but the cavity cells are of constant shape and size.

Fluent provides three options for dynamic meshing; smoothing, layering and
remeshing. These are explained in *ANSYS FLUENT Theory Guide* [4]. Two or
even all three methods can be applied simultaneously. Regardless of choice of
method, a number of parameters must be specified by the user.

Remeshing can be seen as advantageous where mesh elements are mainly
triangular (in 2D) or tetrahedral (in 3D), whereas smoothing is suitable in

cases of small mesh deformations.

Owing to its capability to maintain a high quality mesh during relatively large deformations, the dynamic layering technique has been selected for the deforming piston zone in the synthetic jet geometry (a time-constant mesh is kept for the main geometry). An initial mesh, displayed in Figure 4.1 was constructed with quadrilateral elements in the piston region.
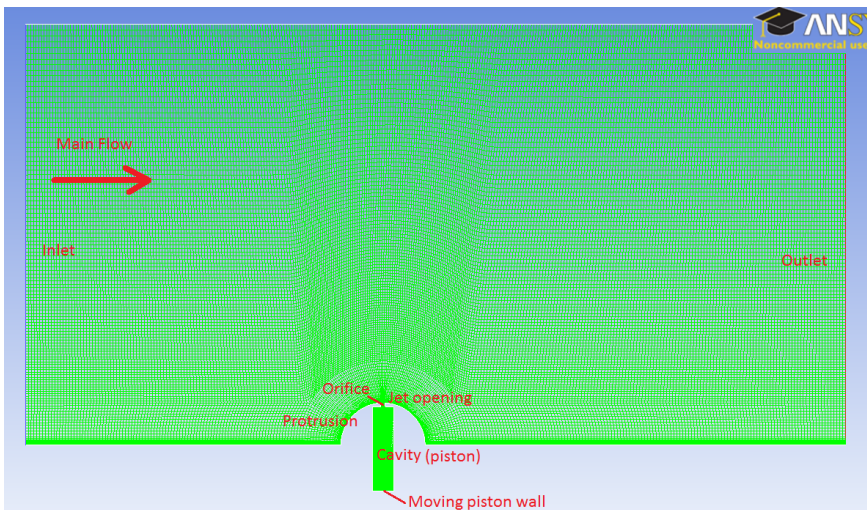


**Figure 4.1:** Mesh

Layering causes new layers of quadrilateral cells to develop in the cavity during the piston suction stroke. Correspondingly, layers of cells collapse during the blowing stroke. Thus, problems with negative volume cells is eliminated. Fluent enables the user to control the emerge and collapse of layers by specifying maximum layer height. Once exceeding this limit, a new layer is constructed.

Figure 4.2 displays snapshots of the mesh. The lower wall of the cylinder has moved a vertical distance of 10 mm downwards between the two pictures. A user-specified layer height tolerance of maximum 2 mm has caused five new mesh layers to form.
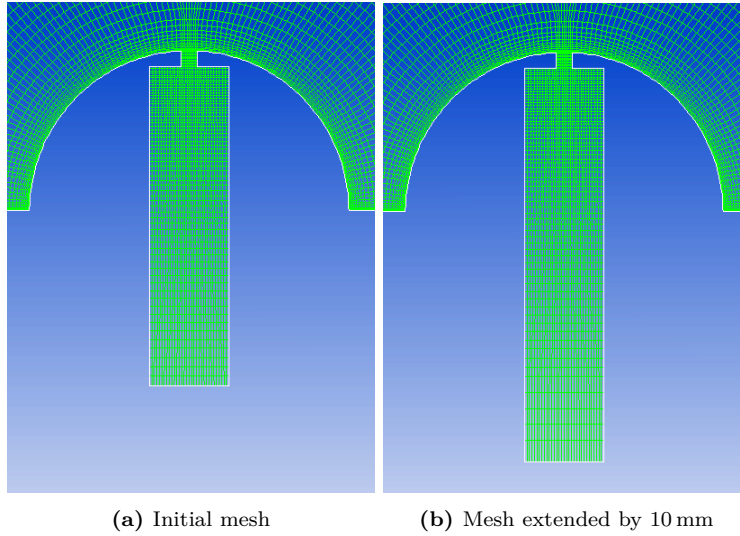
(a) Initial mesh                    (b) Mesh extended by 10 mm

**Figure 4.2:** Dynamic mesh.    Illustration of the "layering" mesh update
technique, where new layers of quadrilateral cells grow or collapse
at the moving boundary.

## 4.4   Boundary conditions

Fluent requires the user to define boundary conditions at suitable locations.
As it is interesting to investigate how the system responds to change in inlet
velocity for a given frequency and amplitude, the boundary type "Inlet velocity"
is chosen. Here, the user determines a velocity magnitude to be imposed normal
to the boundary. This case is run for two inlet velocities; namely $1\,\text{m/s}$ and
$10\,\text{m/s}$.

The outlet is modelled as an "Outflow" boundary. Generally, outlet boundaries
can be modelled as outflows with few issues in incompressible flow problems.

Finally, all walls are treated as no slip walls.

## 4.5 UDFs for modelling piston motion

The CFD software Fluent provides the user with extensive control of the CFD model by the so-called User Defined Functions (UDFs) which can be loaded into a Fluent case. UDFs are commonly used when none of the built-in Fluent functions serve the user's needs. In the case of the synthetic jet, the built-in "In Piston" function is sufficient, however, UDFs allows for more flexibility and better control. Therefore, it was chosen to model the piston motion by writing a UDF code.

UDFs are separate text files written in the C programming language. In addition, a range of macros and data structures for Fluent-specific purposes, e.g. for looping through the nodes or cell centres of a mesh edge or face, are listed in *ANSYS FLUENT UDF Manual* [5]. There is also a set of macros available to describe the motion of a dynamic mesh.

In his master thesis, Nøttveit [34] developed a C code for a piston pump comprising seven pistons moving vertically with a phase lag of $360°/7$. Nøttveit's code has served as a basis for the synthetic jet case, however, a number of adjustments were required.

The Fluent macros `DEFINE_GRID_MOTION`, `NOD_POS_NEED_UPDATE` and `NODE_POS_UPDATED` are crucial elements in the code, together with a sine function that dictates the displacement of the grid at each time step.

The bottom wall of the piston is modelled as a moving wall, following a sine function. At each time step, the vertical displacement of the mesh is calculated from $\Delta y(t) = v(t)\Delta t$. The displacement is added to the previous mesh position using the `NV_V_VS` macro in order to obtain an updated position for the lower piston wall.

$$y(t) = \Delta h \sin(\omega t) \tag{4.1}$$

and

$$v(t) = \frac{d}{dt} y(t) \Rightarrow v(t) = \Delta h \cdot \omega \cos(\omega t) \tag{4.2}$$

Accordingly,

$$\Delta y(t) = \Delta h \cdot \omega \cdot \Delta t \cos(\omega t) \tag{4.3}$$

The variables `time` and `dtime` in the corresponding UDF code line

```
displ=-dtime*2*3.14*freq*amp*sin(2*3.14*freq*time);
```

are automatically passed from Fluent during a simulation run. The complete C-code is given in Appendix B.

## 4.6   Turbulence model

The physics of the synthetic jet problem needs to be considered before choosing a turbulence model. Because the system includes a surface protrusion, separating and reattaching flow can be expected downstream of the protrusion. Also, the synthetic jet itself is expected to produce a significant amount of swirl.

From Fernandino [16], it is known that the $k - \omega$ turbulence model gives more correct results than the $k - \epsilon$ model in separation and reattachment regions of the flow. For swirling flows, the $k - \omega$ model is also generally a good option. Next, Li [27] refers to a number of papers comparing experimental results with numerical simulations of synthetic jets. He concludes that the SST $k - \omega$ turbulence model appears as the most favourable choice for CFD simulations of synthetic jets. Finally, the two-equation $k - \omega$ model is not among the most computationally expensive available. The knowledge from Fernandino [16] and Li [27] justifies the use of the SST $k - \omega$ model for the systen under investigation.

## 4.7   Numerical scheme

First order numerical methods are less time-consuming than higher order methods, while higher order methods can provide higher accuracy.  This trade-off needs to be considered when choosing which numerical scheme to use. Here, the desire to run as many as 42 CFD analyses has outweighed the need for a more precise numerical scheme. Hence, first order methods was chosen to discretise both space and time derivatives of Equations 2.2 and 2.3

## 4.8 Time step and simulation time

For all simulations, fixed time stepping is used. A time step corresponding to 1000 time steps per cycle is believed to resolve the motion sufficiently in time. The time step length depends on the oscillation frequency of the case:

$$\Delta t = \frac{1}{f \cdot 1000} \tag{4.4}$$

This is well below the maximum time step reported in literature for similar CFD cases. For example, Mane et al. [30] has given the time step as

$$\Delta t = \frac{1}{f \cdot 200} \tag{4.5}$$

No criterion restricts the number of iterations within one time step before advancing to the next time step. 20 iterations (the maximum number of iterations allowed by Fluent) are run for each time step, independent of residual values.

All simulations are run for 5000 time steps, which equals five full cycles of piston motion.

## 4.9 Parameter study

Fluent cases are run for combinations of the following parameters:

| Parameter | | Values |
|---|---|---|
| Frequency of piston motion | $f$ | 1, 5, 10, 50, 100, 500, 1000 Hz |
| Amplitude of piston stroke | $\Delta h_0$ | 0.02, 0.04, 0.06 m |
| Velocity of main flow | $U_\infty$ | 1, 10 m/s |

**Table 4.1:** Parameters in Fluent cases

This sums up to $7 \times 3 \times 2 = 42$ combinations.

# Chapter 5

# Components in a mechanical resonance system

As discussed in Section 3.1, the synthetic jet system should be operated at resonance in order to reduce the energy consumption of the actuation system. This chapter will look into possible practical methods to drive the system, and technologies to vary spring stiffness.

The actuation system must be capable of providing a driving force which enforces time-varying displacement of the piston wall as given in Equation 3.1. Also, stiffness needs to be tuned in accordance with Equation 3.9 when added mass changes. As previously explained, the objective of altering spring stiffness is to ensure that the excitation force is kept at a frequency equal (or close) to the natural frequency of the system.

Recent developments in materials engineering have increased the number of possible solutions for both actuation systems and variable stiffness springs. In the following, both conventional and more novel solutions will be described.

It should be noted that no designs are found for hydro power applications or flow control of liquids. Most of the solutions described in the following are developed for automotive or aerospace applications.

## 5.1    Fundamentals of smart materials

In this context, the term "smart materials" refers to materials with provide displacement in response to electric fields, magnetic fields or temperature. All theory on piezoelectric materials and Shape Memory Alloys in the following two subsections can be found in Jalili [23] and Schwartz [38].

### 5.1.1    Piezoelectric materials

Piezoelectric materials exhibit a coupling between mechanical stress/strain and electricity. This effect is named differently depending on whether stress/strain or electric charge acts as input or output. The so-called "direct effect" refers to the phenomena where electric charge is produced in response to mechanical stress/strain (displacement). For actuation purposes, the "converse effect", where electrical charge results in displacement, is more relevant.

Piezoelectric materials occur in nature, examples include bone, quartz and paraffin. Synthetic materials have been developed to obtain properties useful for industrial purposes. Among the most common synthetic piezoelectric materials are titanates, e.g. lead zirconate titanate (PZT) or barium titanate.

### 5.1.2    Shape Memory Alloys

Shape Memory Alloys (SMAs) can appear in one of two different crystalline phases - martensite and austenite - where the martensitic phase is softer than the austenitic phase. The two phases are associated with different shapes. Hence, a transformation between the two phases will cause displacement. The "shape memory" effect refers to a SMA's ability to switch between the two phases/shapes by applying heating or cooling. The transformation temperature strongly depends on the SMA material. When transforming back and forth between the two phases, hysteresis will become an issue. Nickel-titanium and other nickel-based alloys are known to exhibit a low degree of hysteresis and are commonly used in industry. Alternatively, copper-based SMAs are also commercially available.

SMAs are capable of generating relatively high power output relative to their weight. Schwartz [38] emphasises that their reliability in the long run is not

well documented, especially when it comes to material cracking after a number of transformation cycles.

## 5.2 Linear actuator

The synthetic jet system requires a linear driving force in order to obtain the oscillations of the piston wall (or diaphragm). For this purpose, two groups of motors are available; rotary-to-linear motion conversion motors and direct linear drive motors. In this thesis, emphasis will be placed on the latter group.

The choice of motor should be based upon performance requirements. The various sub-groups of linear motors possess different qualities, such as precision, stroke length, maximum speed and reliability.

A characteristic of linear actuators is that force, rather than torque, is transmitted. Several variants of linear electric motors exist, the most relevant are described in Bolton [8] and listed below:

- Stepper motor

- DC Brush motor

- Voice coil motor

- Synchronous motor

- Induction motor

Additionally, options using smart materials include

- Piezoelectrically driven diaphragm

- SMA driven diaphragm

Here, three examples of actuator systems for synthetic jets found in literature will be given. First, the linear electric motors are represented by a conventional voice-coil motor. Both variants of smart material actuators will also be described.

## Voice coil motor

The voice coil motor is a linear actuator which, under influence of a constant magnetic flux density, provides a force proportional to electric current. The following relation can be found in Chen et al. [11]:

$$\mathbf{F} = l\mathbf{I} \times \mathbf{B} \tag{5.1}$$

Chen et al. [11] claimed that the voice coil motor is suitable for a diverse range of engineering applications due to its small size and high force-to-weight ratio.

McCormick et al. [31] designed an actuation system for a full-scale synthetic jet built for aircraft applications. The authors aimed at increasing the stall angle by 5 degrees and the lift coefficient by 10% by introducing a synthetic jet of frequency 250 Hz and maximum velocity 65 m/s. Although a piezoelectric solution was an option, a conventional voice coil motor was selected. The reasons to choose a voice coil motor are given by McCormick et al. [31] as low weight, small size and commercial availability together with sufficient performance.

## Piezoelectrically driven diaphragm

The use of oscillating diaphragms made of piezoelectric materials is a more novel technique which can be used to produce synthetic jets. Mane [29] investigated three piezoelectric diaphragms of various piezoelectric materials but concluded that variations between the three types in this experiment were not statistically significant. On the other hand, the shape of the waveform of the signal imposed on the diaphragm proved significant. Signals of "saw-tooth" or square shape caused higher maximum jet velocity than sine signals.

The work by Ugrina and Flatau [42] describes design and frequency tuning of piezoelectrically driven synthetic air jets. Although their article is focused on altering mass rather than stiffness in order to obtain the desired resonance frequency, aspects of diaphragm and cavity design are of interest for the design of a piezoelectrically driven synthetic water jet. The shape and thickness-to-diameter ratio of the diaphragm are observed to be influential parameters. Square-shaped diaphragms perform better than circular ones. Next, an optimal thickness-to-diameter ratio of 0.17 is found. It is not discussed whether the optimal ratio is valid for air jets only.

Conventional piezoelectric actuators can only provide displacements of a few millimetres. The so-called recurve actuator can be utilized when larger diaphragm displacement is required. An investigation of a recurve piezoelectric actuator is presented in Gravatt and Flatau [20]. Experiments proved that their objective; to obtain a 30 m/s jet for a frequency of 100 Hz, was possible.

### SMA driven diaphragm

Piezoelectrically driven synthetic jets have so far not exceeded 300 Hz or 100 m/s. According to Liang et al. [28], strong synthetic jets can be achieved with the use of ferromagnetic shape memory alloy (FSMA) composites as actuators. Strong jets are developed for high-performance applications, e.g. high Mach number flights. The ferromagnetic material, in the case of Liang et al. [28] a nickel-titanium alloy, can be manufactured as a thin and elastic diaphragm. Oscillations which are induced by an electromagnet, are observed by Liang et al. to have a maximum stroke length of 3.72 mm and velocity 190 m/s.

## 5.3 Variable stiffness springs

As described in Section 3.1, a variable stiffness spring need also be included in the synthetic jet system. A variable stiffness spring makes manipulation of the system's resonance frequency possible.

### 5.3.1 Conventional springs

Cronjé et al. [12] described several methods to obtain variable stiffness springs. A summary of possible methods is given below.

### Leaf springs

Leaf springs are based on the principle that spring stiffness increases with increasing tension. A schematic is shown in Figure 5.1. When the the two metal "leaves" are separated by an external force, tension increases. Hence, this

deflection increases spring stiffness. The relation between leaf separation and effective stiffness must be known.

One may assume that a piezoelectric or shape memory alloy actuator could provide the force required to separate the leaves.
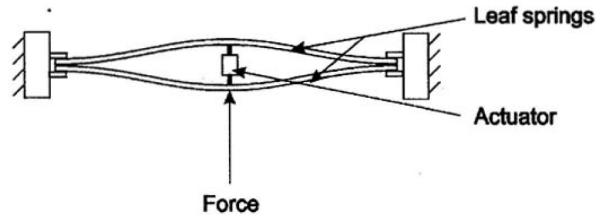


**Figure 5.1:** Leaf spring with linear actuator between the two leaves. Stiffness increases as the two leaves separate. Figure from [12]

Walsh and Lamancusa [45] were able to increase the stiffness of steel leaf spring similar to that displayed in Figure 5.1 by a factor of 45 when separating the leaves. Both finite element analysis (FEM) and experiments proved that effective stiffness increased linearly with separation. A non-linear relation between separation and stiffness was demonstrated for further increase in separation.

## Helical springs

The stiffness of helical springs, or coil springs, can be manipulated in a number of ways. A derivation of the spring constant for a helical spring, based on strain energy considerations and Castigliano's theorem, can be found on page 402 in Gambhir [18]. The result is given below:

$$k = \frac{Gd^4}{8D^3N} \tag{5.2}$$

During the operation of a mechanical system, the most obvious variable to change will be the number of active coils, $N$. One possible arrangement is described by Ramaratnam and Jalili [35]. Here, an external metal arm can be

used to block the coils at specific locations, so that only a prescribed portion of the total number of coils is free to deflect.

Equation 5.2 is valid provided that the spring is aligned along the same axis as the force applied to the spring. Hence, another option is to adjust $k$ by changing the angle of the spring axis.

### 5.3.2 Smart springs and combination of different springs

Piezoelectric materials exhibit different stiffness when in short and open circuit and can hence be used directly as variable stiffness springs. Similarly, the stiffness of SMA springs depends on whether the material is in martensite or austenite phase.
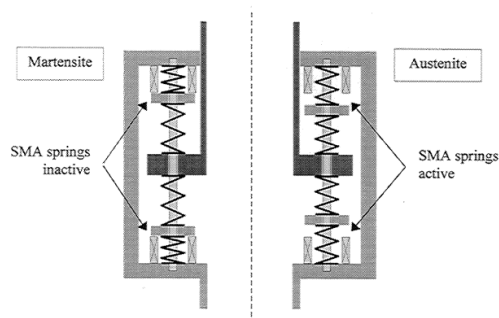


**Figure 5.2:** Variable stiffness spring with SMA actuator. Figure from [39]

A system using SMA springs is described by Siler and Demoret [39] and displayed in Figure 5.2. Here, a standard steel coil spring is combined with a SMA coil spring. The nickel-titanium (NiTi) alloy SMA spring is active when in austenite phase and passive in martensite phase. As seen from Figure 5.2, the two springs are connected in series. Equivalent spring stiffness for a serial connection of $n$ springs is given in Schmitz and Smith [37] as

$$\frac{1}{k_{eq}} = \sum_{j=1}^{N} \frac{1}{k_j} \qquad (5.3)$$

From Equation 5.3 it can be seen that austenite phase corresponds to a lower

overall stiffness. Siler and Demoret [39] reported that stiffness could be reduced by 70 % by combining a standard steel coil spring with a SMA coil springs in as shown in Figure 5.2.

Nevertheless, the most common variable stiffness springs utilising smart materials are variants of the "Smart Spring" patented in 1999 by Prof. Fred Nitzsche at Carleton University, Canada. Here, smart materials are used as actuators built-in in a spring system rather than acting as springs themselves.
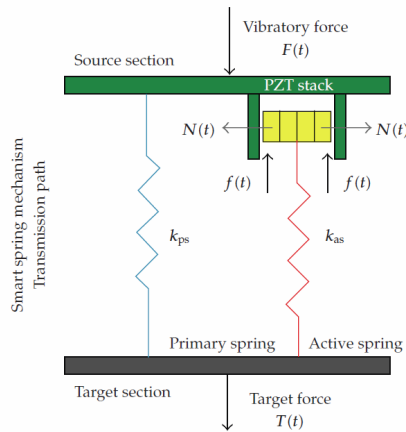


**Figure 5.3:** Smart Spring Mechanism. Figure from [10]

A schematic of the Smart Spring system is displayed in Figure 5.3. The system is described in e.g. Nitzsche et al. [33] as a combination of two mass-spring systems. A primary spring with stiffness $k_1$ is always active, while a secondary spring with stiffness $k_2$ can be attached using a piezoelectric actuator.

When the secondary spring is passive, there is a small gap between the piezoelectric stack and the reinforcements on each side of the stack. Imposing a voltage to the piezoelectric stack leads to an expansion which eventually closes the gap so that a frictional force between the stack and reinforcements becomes present. Hence, the secondary spring becomes coupled with primary spring.

The frictional force can be expressed as

$$F_{friction} = \nu N \tag{5.4}$$

where $\nu$ is the material-dependent coefficient of friction and $N$ is the normal force. Nitzsche et al. [33] reported that the stiffness of the secondary spring is directly proportional to the voltage applied to the actuator.

For a combination of $n$ springs in series, the equivalent spring stiffness can be found in e.g. Schmitz and Smith [37] as

$$k_{eq} = \sum_{j=1}^{N} k_j \tag{5.5}$$

According to Equation 5.5, stiffness can be varied between a minimum $k_1$ and a maximum $k_1 + k_2$ for the Smart Spring case with two springs.

The original system as described in Nitzsche et al. [33] suggest the use of a piezoelectric actuator. Variants of the Smart Springs with SMA actuators may also be used. Regardless of choice of actuator, relatively low force and micro displacement is sufficient to obtain the desired effect.

Although the topic of control engineering is not highlighted here, one should bear in mind that the the operation of a variable stiffness spring requires a control system. Acceleration, velocity or displacement should be measured by sensors. Emphasis must be placed on the degree of stiffness change and response time required for successful operation of the system.

# Chapter 6

# Results and discussion

The overall objective of this study has been to investigate added mass effects in liquid flow. This chapter will present results obtained from analytic and numerical analysis.

## 6.1 Validation of CFD simulations

As no experimental data is available for validation, CFD results will be validated against the analytic model outlined in Chapter 3. Non-dimensionalised added mass for all CFD cases is displayed in Figure 6.1. Added mass has been non-dimensionalised using the frequency and amplitude-independent analytic added mass (Equation 3.10) as a reference. Frequency has not been non-dimensionalised in order to simplify comparison with the Bode plot in Figure 6.2.

As described in Section 4.9, simulations were initially run for frequencies 1, 10, 100 and 1000 Hz and then filled in with in 5, 50 and 500 Hz. Preliminary results obtained from this range of frequencies suggested that added mass displayed an interesting trend between 1 and 5 Hz for $U_\infty = 1\,\text{m/s}$, and between 10 and 100 Hz for $U_\infty = 10\,\text{m/s}$. Here, added mass obtained from CFD appears to plummet, in some cases even below analytic added mass. New runs of simulations were carried out at $2\,\text{Hz}$ for $U_\infty = 1\,\text{m/s}$, and 25 and $75\,\text{Hz}$ for $U_\infty = 10\,\text{m/s}$ to complete the picture.
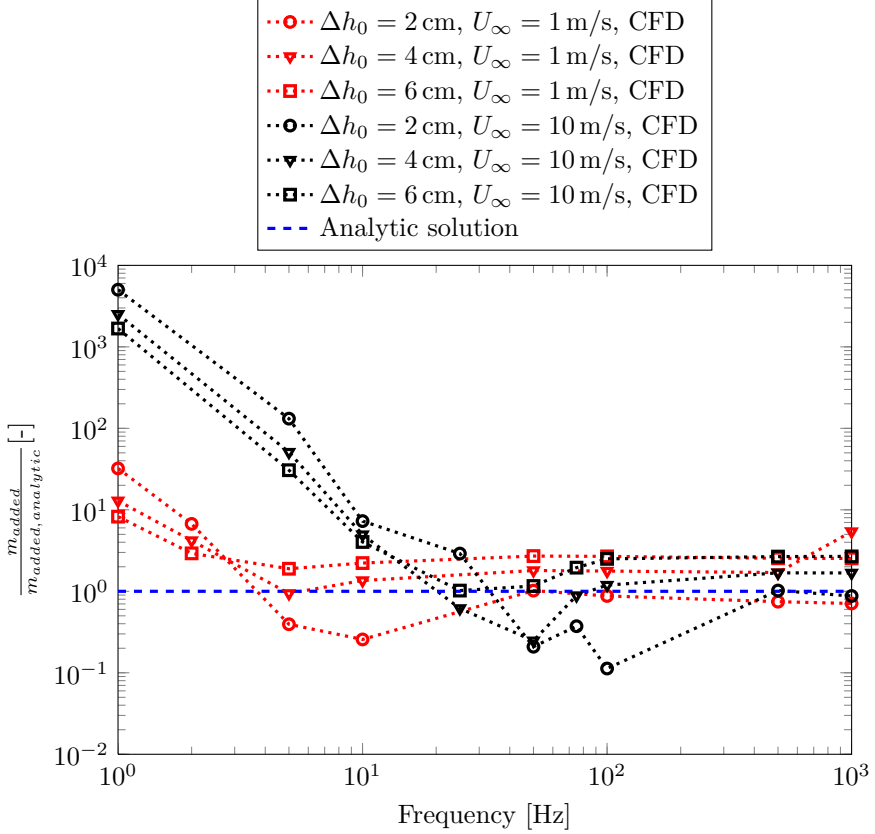
**Figure 6.1:** Added mass

Lower added mass than expected in a limited frequency range is interpreted as an evidence of resonance frequencies of the synthetic jet system. This could be due to the development of self-sustaining pressure fluctuations as explained in Section 2.1.4 or other pressure variations occurring at frequencies equal to frequencies where low added mass is observed. Kuo and Jeng [25] proved that self-sustaining pressure fluctuations across a cavity are present in water. Interaction between the excitation frequency and frequency of self-sustaining pressure oscillations might establish an instability which contributes to resonance. Similarly, separation and vortex shedding downstream of the

synthetic jet, due to the surface protrusion, might also affect the system.

From Figure 6.1, one can observe that increasing $U_\infty$ is associated with a rightwards shift in the region of resonance frequency. One should bear in mind that the result rely on a limited number of CFD simulations, nevertheless, the trend is clearly observed in all CFD cases. More CFD runs for variations in $U_\infty$ can reveal if there is a systematic relation between $U_\infty$ and resonance frequency.

In order to investigate this possible explanation more thoroughly, new simulations where pressure is monitored along a line across the orifice opening should be run. A FFT analysis can reveal if frequency peaks in the regions of interest.

For frequencies higher than those defining the resonance regions, CFD results approach an asymptotic added mass value slightly higher than the analytic solution (except for one CFD series). Obviously, the analytic solution is based on a highly simplified model which does only take the geometry of the piston into account. Nonetheless, deviations may also be introduced from the Fourier-average method (Section 3.2) which has been used to calculate added mass from the CFD results. In the Fourier-average method, all forces in phase with acceleration are by definition components of the added mass force. If the pressure force has a component in phase with acceleration, this force will be included as a component of the added mass force, even if its origin is instabilities in the shear layer rather than the added mass phenomenon itself.

The frequency response and phase angle of the dynamic system as given in Figure 3.3 and Equation 3.28 is displayed in Figure 6.2 and 6.3, where the vertical axis in Figure 6.2 represents the gain $|x(j\omega)/F(j\omega)|$ and the vertical axis in Figure 6.3 represents phase angle. From Equation 3.28, it is evident that several parameters influence the solution - some of which have been estimated in Table 3.1. Regions of high gain in Figure 6.2 correspond to regions of low added mass in Figure 6.1.

While analytic added mass as seen in Figure 6.1 is independent of piston frequency and amplitude, analytic frequency response is not. This is due to the fact that $|U_{RMS}|$ increases with increasing $\omega$ and $\Delta h_0$ and vice versa.

There is no doubt that the frequency response analysis heavily relies on assumptions and incomplete information. Nevertheless, the framework and model can serve as a foundation from which trends can be observed.
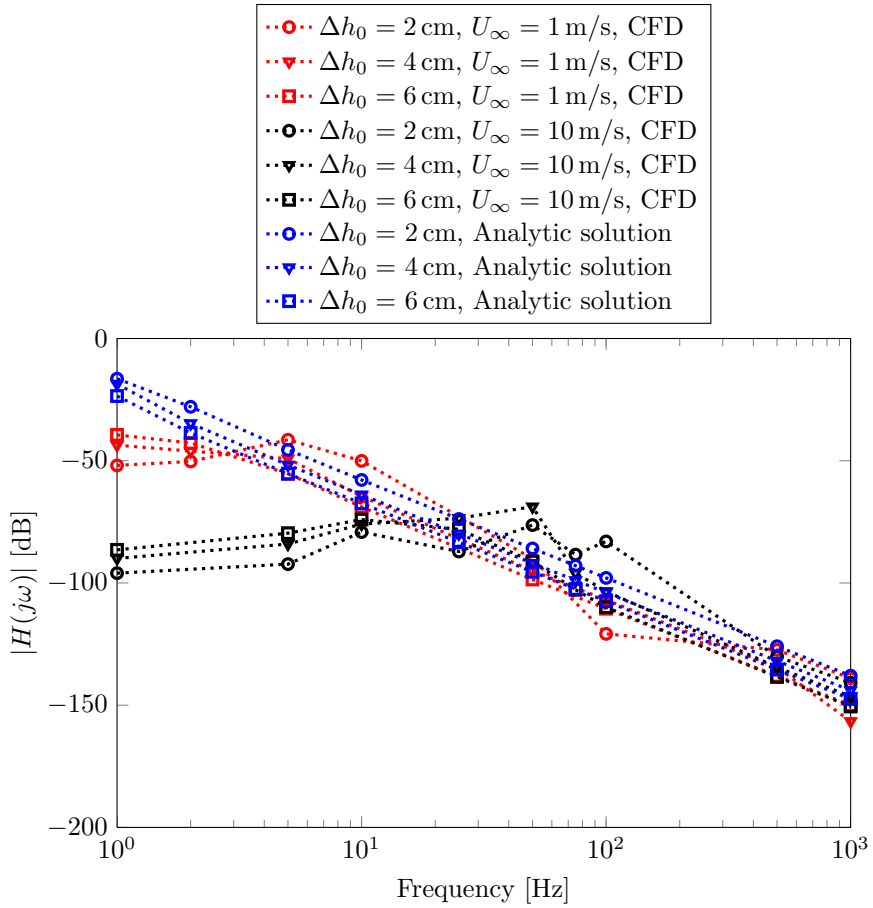
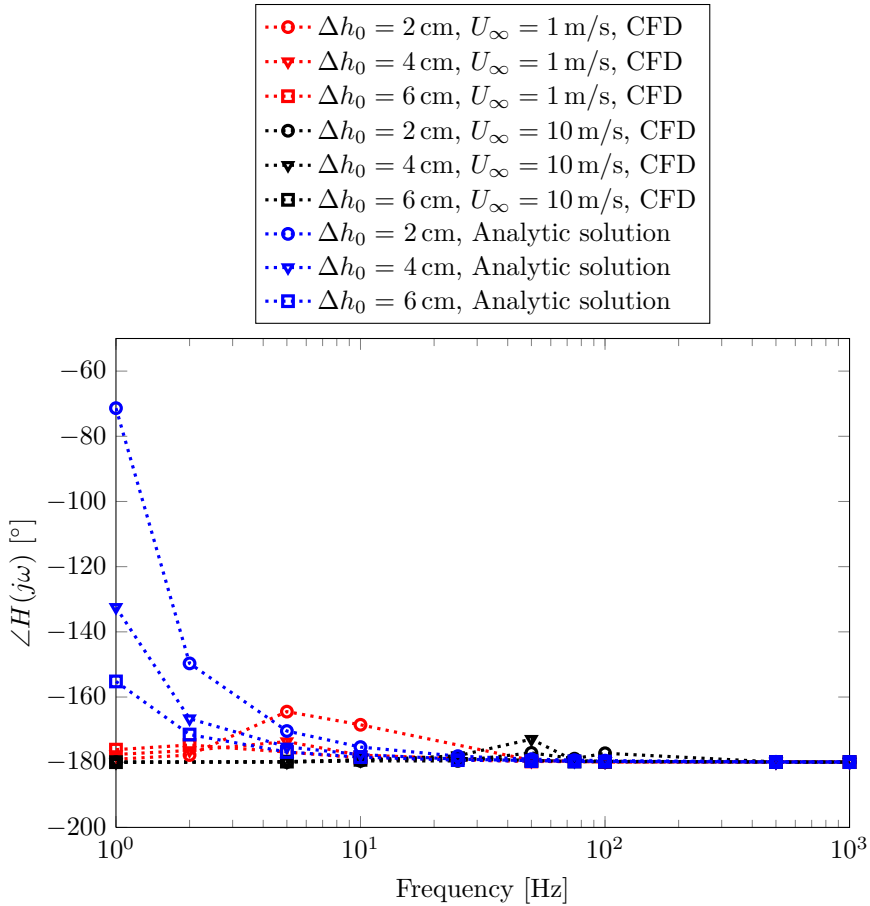**Figure 6.2:** Frequency response of dynamic system for synthetic jet

**Figure 6.3:** Phase angle of dynamic system for synthetic jet

## 6.2   Flow visualisation

### 6.2.1   Streamlines and separation

Figure 6.4 shows the separation bubble which develops downstream of the orifice exit. This effect arises because the flow experiences large curvature. Although flow control devices aim at eliminating vortex shedding, the synthetic jet has not been capable of eliminating the vortex shedding in this case. Similar streamlines can be generated for other operation points.
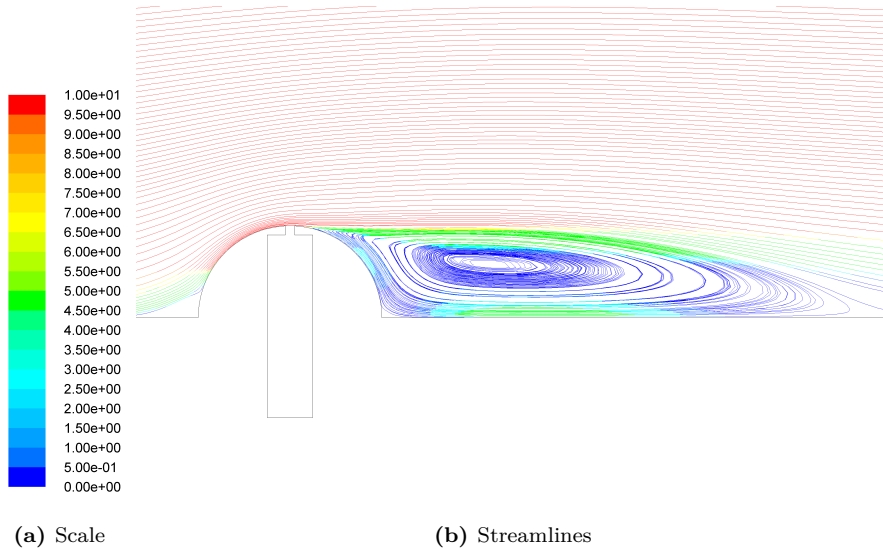


**(a)** Scale                          **(b)** Streamlines

**Figure 6.4:** Streamlines for $f = 0\,\text{Hz}$ , i.e. inactive synthetic jet

In order to investigate the separation phenomenon more closely, a series of CFD runs were set up for $f = 0, 1, 5, 10, 25$ and $50\,\text{Hz}$, with a monitor recording shear stress in all grid points along the surface protrusion for every time step. A function searching through the shear stress arrays for the $x-$coordinate at which the shear stress changed sign, was used to locate separation points for each of the frequencies.

For $f = 0\,\text{Hz}$, where the synthetic jet was inactive, a steady separation point was identified at $x = 5.2\,\text{mm}$ ($x = 0$ is defined in the centre of the piston - increasing

positive $x$-coordinate corresponds to a position further downstream of the orifice exit). However, when employing the synthetic jet, the separation point displayed an unsteady behaviour and travelled back and forth along the protrusion surface. Although its location varied with $\omega$, the average location of the separation point was downstream of the separation point for $f = 0\,\mathrm{Hz}$. Hence, Figure 6.5 displays that the synthetic jet fulfils one of the two objectives presented in Section 2.3: Separation is delayed, but the location of the separation point is not stabilised. Although the average separation position is located downstream of the steady separation point, fluctuations occur upstream of the steady separation point for all $f > 0\,\mathrm{Hz}$.
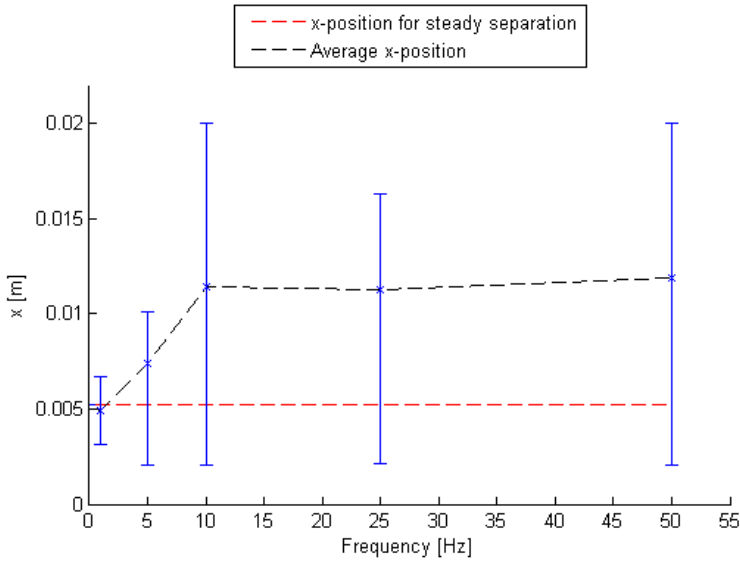


**Figure 6.5:** Average $x$-location of separation points (black line), blue errorbars representing maximum and minimum $x$-location. Red line represents the steady $x$-position when the synthetic jet system is inactive.

### 6.2.2   Vorticity contour plot

Figures 6.6b to 6.6f display vorticity contours for an arbitrary CFD case in order
to display the formation and evolution of the jet. The snapshots are taken for
various $t/T$ for the last duty cycle of a simulation with a total of five duty cycles,
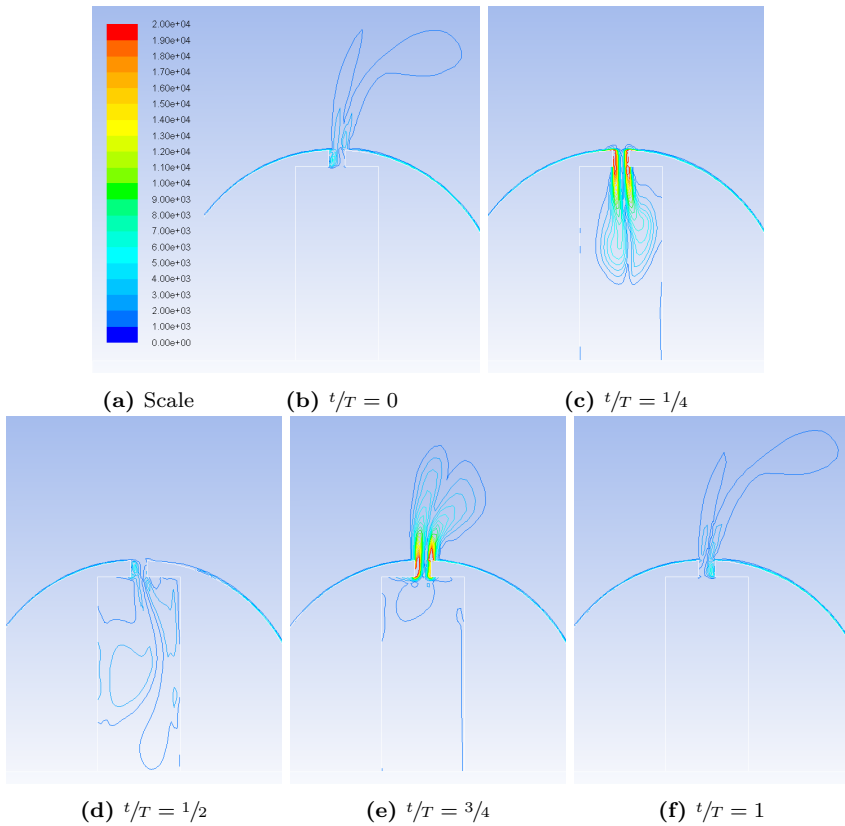in order to minimise impact from start-up effects.



**(a)** Scale          **(b)** $t/T = 0$          **(c)** $t/T = {}^{1}/_{4}$

**(d)** $t/T = {}^{1}/_{2}$          **(e)** $t/T = {}^{3}/_{4}$          **(f)** $t/T = 1$

**Figure 6.6:**  Vorticity contour plot for one duty cycle.
Here, $f = 50\,\text{Hz}, \Delta h_0 = 4\,\text{cm}, U_\infty = 1\,\text{m/s}$

In Figure 6.6, the jet is not sufficiently strong for the vortices to detach from the
surface. The conditions for the vortex pair to detach has not been systematically

investigated, but Figure 6.7 indicates that the excitation frequency contributes. Except that $f = 500\,\mathrm{Hz}$ in Figure 6.7, flow conditions are similar for Figure 6.6f and Figure 6.7.
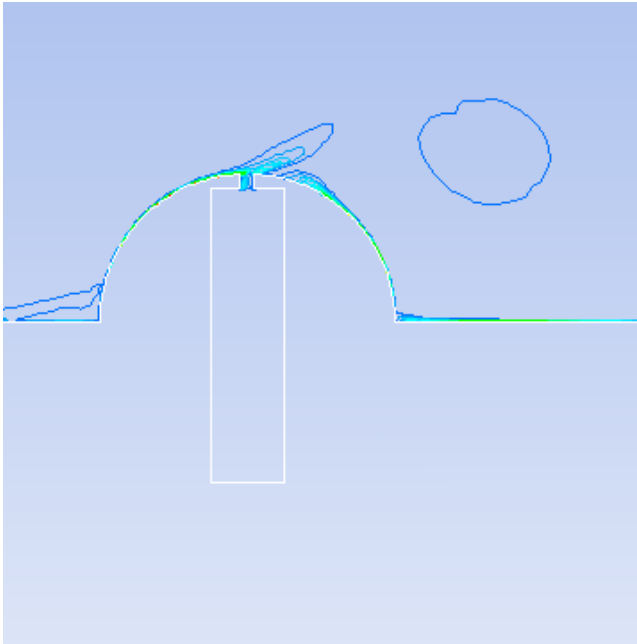


**Figure 6.7:** Detached vortex ring, drifting downstream. Here, $t/T = 1, f = 500\,\mathrm{Hz}, \Delta h_0 = 4\,\mathrm{cm}, U_\infty = 1\,\mathrm{m/s}$

## 6.3 Verification of CFD simulations

In this thesis, focus has not been on achieving the most exact representation of the system. Therefore, simulations have been run using a grid which is believed to have sufficient spatial resolution. Neither systematic grid nor timestep convergence analyses have been conducted. However, it has been ensured that the non-dimensional height of grid layer closest to the solid surface, $y+$, is within the SST $k - \omega$ turbulence model limits, that the time step is reasonable when the case is compared with similar known studies

(Section 4.8) and that low residual values are achieved at every time step in the transient simulations. It is well known that a first order numerical scheme is less accurate than schemes of higher order. Here, a first order scheme was chosen because higher order schemes were too time-consuming. Although choice of discretization scheme is not believed to have a major impact on the results, it should be regarded as a possible source of inaccuracy.

When drawing the CFD geometry, the domain was extended far up- and downstream of the synthetic jet in order to reduce the probability for inlet and outlet boundaries to affect the solution. Boundary conditions shall generally not be imposed in regions of steep gradients. As seen from Figure 6.8, the inlet and outlet are not located in or close to steep gradient regions. Similar figures can be obtained for other variables as pressure and vorticity, and for other values of $\Delta h_0, U_\infty, f$ and $t/T$.

Generally, turbulence models might have an impact on the CFD solution. In the case of the synthetic jet, the turbulence model is assumed to have most influence on the results related to separation and location of separation points, where the dynamics in the boundary layer are important.

Finally, it should be noted that the entire numerical analysis has only ben conducted in 2D. Hence, three-dimensional effects in the flow cannot be accounted for.
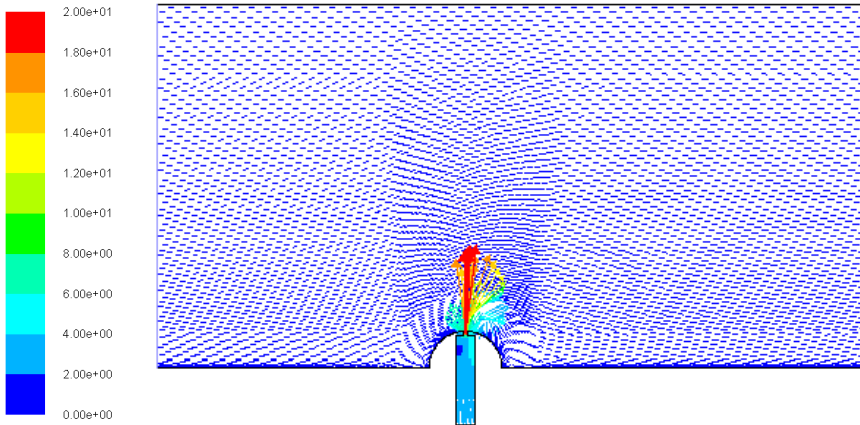
**Figure 6.8:** Velocity scale in (a) with unit m/s. Velocity vectors in (b) are displayed for the entire computational domain. Inlet (left) and outlet (right) show no evidence of strong velocity gradients. Here, $\Delta h_0 = 6\,\mathrm{cm}$, $U_\infty = 1\,\mathrm{m/s}$, $f, = 50\,\mathrm{Hz}$, $t/T = 0.75$

## 6.4 Energy requirements of a synthetic jet actuation system

Added mass has demonstrated a reduction in local frequency ranges. It is desirable to operate the system here. It is also possible that other effects will introduce additional energy requirements which are not considered in the CFD model. The lower piston wall has been modelled as a rigid wall in CFD simulation. In a realistic synthetic jet, that wall is likely to be a flexible piezoelectric or SMA membrane that allows for deformation, which presumably adds to the energy requirement of the system.

Next, the nozzle in the CFD geometry has not been designed for minimum losses. As nozzle losses are proportional to $v^2$, losses can become considerable at least if the system will be operated at high frequencies. $K_n$ can be significantly reduced if more care is taken while designing the orifice

## 6.5   Synthetic jets in a hydro power context

In this study, the synthetic jet has been applied to a 2D pipe flow where flow conditions might be quite different from draft tube flow. The simulations conducted here cannot predict whether - or how - a rotating vortex rope which occurs in draft tubes in power plants running one part load (see section 2.5) influence the flow.

When it comes to loss of water, the synthetic jet is beneficial compared to the injection system described in 2.5. Conversely from Francke's injection system, synthetic jets require no water to be bled off upstream of the turbine.

## 6.6   Choice of components for synthetic jet system

For the variable stiffness spring, the most promising techniques seem to be the Smart Spring or the leaf spring combined with a piezoelectric or SMA actuator. These two systems can provide continuous variation of stiffness between a lower and an upper limit, while they are also relatively compact and lightweight.

For the choice of actuator, a linear voice-coil motor would most likely serve the needs of an actuation system at the Hydro Power Laboratory. However, this thesis has not investigated the effect of synthetic jets operating with short displacement. If the desired effect can be obtained with displacement in the order of less than a centimeter, a piezoelectric diaphragm is a realistic option.

# Chapter 7

# Conclusion

Injecting a pulsating synthetic jet into a main flow can be classified as an active flow control technique. The most frequently reported examples of applications of synthetic jets are found in military aircrafts. Generally, synthetic jets in gas flows are more thoroughly investigated than in liquid flows.

One possible future application of water synthetic jets is in hydro turbine draft tube flow. In this study, added mass and frequency response of a synthetic water jet has been investigated through analytic analysis and CFD simulations using a dynamic grid. A main interest has been whether certain resonance frequencies could be identified. It is desirable to operate the system at resonance in order to reduce power consumption of the excitation force driving the system.

Added mass has been calculated from CFD simulation results using the Fourier-Average method. For a given piston geometry, analytic added mass was constant while added mass from CFD showed dependence of $\Delta h_0, U_\infty$ and $\omega$, which cannot be explained from the analytic solution. The same dependence is found from the frequency response analysis, where the resonance frequency regions of low added mass correspond to high gain in the Bode diagram.

Although the resonance behaviour has not been fully understood, one possible explanation is a resonance phenomenon where the piston excitation frequency coincides with the frequency of self-sustaining pressure oscillations which are expected to occur across the cavity. Also, separation downstream of the synthetic jet might create a time-varying pressure field which could possibly

contribute to resonant behaviour. The resonance frequency region is observed to move towards higher frequencies for higher free-stream Reynolds number. This is in agreement with the behaviour of the frequency of self-sustaining pressure oscillations known from literature.

Although less effort was placed on assessing the synthetic jet's impact on boundary layer separation, one exception was made for a series of simulations for a given $\Delta h_0$ and $U_\infty$. Results indicate that the separation point is steady as long as the jet is inactive. Once the jet is employed, the separation points becomes unstable, though with an average $x$-location downstream of the steady $x$-location.

It has been demonstrated analytically that manipulation of $\omega$ requires a varying stiffness spring in the system, so that operation at resonance is achieved. For a prospective laboratory rig at NTNU, the patented "Smart Spring" is suggested for this purpose. A linear voice coil motor is recommended for driving the system.

# Chapter 8

# Further work

In order to better understand the apparent resonance effect, it would be beneficial to re-run the simulations with pressure monitors set up at locations of interest - namely across the orifice and along the surface protrusion. This will enhance the quality the results, as the effects influencing the resonance frequency regions can be isolated and described.

This CFD study has aimed at describing trends and patterns which can be expected to find in the system under investigation. Experimental results from a laboratory rig will give invaluable information if more detailed knowledge of the system is desired.

# Bibliography

[1]  D. G. Akhmetov. *Vortex rings*. 2009. URL: http://www.worldcat.org/isbn/9783642050152.

[2]  M. Amitay and A. Glezer. "Aerodynamic Flow Control Using Synthetic Jet Actuators Control of Fluid Flow". Ed. by P. Koumoutsakos and I. Mezic. Vol. 330. Lecture Notes in Control and Information Sciences. Berlin, Heidelberg: Springer Berlin / Heidelberg, 2006. Chap. 2, pp. 45–73. ISBN: 978-3-540-25140-8. DOI: 10.1007/978-3-540-36085-8_2.

[3]  J. D. Anderson. *Fundamentals of aerodynamics*. 5th ed. McGraw-Hill, 2011. ISBN: 9780071289085.

[4]  *ANSYS FLUENT Theory Guide*. 2011.

[5]  *ANSYS FLUENT UDF Manual*. 2011.

[6]  K. H. Aronsen. *An experimental investigation of in-line and combined in-line and cross-flow vortex induced vibrations*. Norwegian University of Science, Technology, Faculty for Engineering Science, and Technology, Marine Technology, 2007. ISBN: 9788247156582.

[7]  J. G. Balchen, T. Andresen, and B. A. Foss. *Reguleringsteknikk*. Institutt for teknisk kybernetikk, NTNU, 2003. ISBN: 8247151472.

[8]  W. Bolton. *Mechatronics : a multidisciplinary approach*. Pearson Prentice Hall, 2008. ISBN: 9780132407632.

[9]  *Boundary layer - Velocity profiles*. URL: http://sci-fix.blogspot.com/2010/08/paragliding-aerodynamics.html.

[10] A. A. Cavalini, T. V. Galavotti, T. S. Morais, E. H. Koroishi, and V. Steffen. "Vibration Attenuation in Rotating Machines Using Smart Spring Mechanism". *Mathematical Problems in Engineering* 2011 (2011), pp. 1–14. DOI: `10.1155/2011/340235`.

[11] Y.-D. Chen, C.-C. Fuh, and P.-C. Tung. "Application of voice coil motors in active dynamic vibration absorbers". *IEEE Transactions on Magnetics* 41.3 (2005), pp. 1149–1154. DOI: `10.1109/TMAG.2004.843329`.

[12] J. M. Cronjé, P. S. Heyns, N. J. Theron, and P. W. Loveday. "Development of a Variable Stiffness and Damping Tunable Vibration Isolator". *Journal of Vibration and Control* 11.3 (2005), pp. 381–396. DOI: `10.1177/1077546305048585`.

[13] J. V. Ekanger. "Morphing Skins to Improve Local Flow Behavior in a Hydroturbine Context". MA thesis. NTNU, 2011.

[14] O. M. Faltinsen. *Sea loads on ships and offshore structures*. Cambridge University Press, 1993. ISBN: 0521458706.

[15] M. Ferlauto and R. Marsilio. "Synthetic Jet Actuator Modeling for Flow Control Applications Computational Fluid Dynamics 2006". *Computational Fluid Dynamics 2006*. Ed. by H. Deconinck and E. Dick. Berlin, Heidelberg: Springer Berlin Heidelberg, 2009. Chap. 90, pp. 573–578. ISBN: 978-3-540-92778-5. DOI: `10.1007/978-3-540-92779-2_90`.

[16] M. Fernandino. "Lecture notes, TEP4545 Fluids Engineering Specialization". 2011.

[17] H. H. Francke. "Increasing Hydro Turbine Operation Range and Efficiencies Using Water Injection in Draft Tubes". PhD thesis. NTNU, 2010. ISBN: 978-82-471-2344-7.

[18] M. L. Gambhir. *Fundamentals of solid mechanics : a treatise on strength of materials*. PHI Learning, 2009. ISBN: 9788120338708.

[19] L. Gomes and W. Crowther. "Towards a Practical Synthetic Jet Actuator for Industrial Scale Flow Control Applications IUTAM Symposium on Flow Control and MEMS". Ed. by J. F. Morrison, D. M. Birch, and P. Lavoie. Vol. 7. IUTAM Bookseries (closed). Dordrecht: Springer Netherlands, 2008. Chap. 12, pp. 111–118. ISBN: 978-1-4020-6857-7. DOI: `10.1007/978-1-4020-6858-4_12`.

[20]  L. Gravatt and A. Flatau. "Resonance-based low-frequency synthetic jet actuator modeling, design and testing". *Smart Structures and Materials 2006*. Vol. 6173. 1. The International Society for Optical Engineering., 2006, pp. 61730L–61730L–10. DOI: 10.1117/12.658816.

[21]  M. Gad-el Hak. *Flow Control*. Cambridge University Press, 2000.

[22]  I. E. Idelchik and M. O. Steinberg. *Handbook of hydraulic resistance*. CRC Press, 1994. ISBN: 0849399084.

[23]  N. Jalili. *Piezoelectric-based vibration-control systems applications to micro/nano sensors and actuators*. 2010. URL: http://www.worldcat.org/isbn/9781441900708.

[24]  E. Kreyszig. *Advanced engineering mathematics*. John Wiley, 2006. ISBN: 9780471728979.

[25]  C. H. Kuo and W. I. Jeng. "Lock-on characteristics of a cavity shear layer". *Journal of Fluids and Structures* 18.6 (2003), pp. 715–728. DOI: 10.1016/j.jfluidstructs.2003.08.020.

[26]  S. B. Lee, A. Seena, and H. J. Sung. "Self-Sustained Oscillations of Turbulent Flow in an Open Cavity". *Journal of Aircraft* 47.3 (2010), pp. 820–834. DOI: 10.2514/1.44823.

[27]  S. Li. "A numerical study of micro synthetic jet and its applications in thermal management". PhD thesis. Georgia Institute of Technology, 2005.

[28]  Y. Liang, Y. Kuga, and M. Taya. "Design of membrane actuator based on ferromagnetic shape memory alloy composite for synthetic jet applications". *Sensors and Actuators A: Physical* 125.2 (2006), pp. 512–518. DOI: 10.1016/j.sna.2005.09.002.

[29]  P. Mane. "Synthetic jets with piezoelectric diaphragms". *Proceedings of SPIE*. San Diego, CA, USA: SPIE, pp. 233–243. DOI: 10.1117/12.599584.

[30]  P. Mane, K. Mossi, A. Rostami, R. Bryant, and N. Castro. "Piezoelectric Actuators as Synthetic Jets: Cavity Dimension Effects". *Journal of Intelligent Material Systems and Structures* 18.11 (2007), pp. 1175–1190. DOI: 10.1177/1045389X06075658.

[31]  D. C. McCormick, S. A. Lozyniak, D. G. MacMartin, and P. F. Lorber. "Compact, high-power boundary layer separation control actuation development". *2001 ASME Fluids Engineering Division Summer Meeting*. 2001.

[32]   M. Nishi, K. Yoshida, and K. Morimitsu. "Control of separation in a conical diffuser by vortex generator jets". *JSME International Journal* 41.1 (1998), pp. 233–238.

[33]   F. Nitzsche, T. Harold, V. K. Wickramashingh, C. Yong, and D. G. Zimcik. "Development of a Maximum Energy Extraction Control for the Smart Spring". *Journal of Intelligent Material Systems and Structures* 16.11-12 (2005), pp. 1057–1066. DOI: `10.1177/1045389X05059964`.

[34]   E. Nøttveit. "Numerisk analyse (CFD) av stempelpumpe". MA thesis. NTNU, 2010.

[35]   A. Ramaratnam and N. Jalili. "A switched stiffness approach for structural vibration control: theory and real-time implementation". *Journal of Sound and Vibration* 291.1-2 (2006), pp. 258–274. DOI: `10.1016/j.jsv.2005.06.012`.

[36]   *Schematic of synthetic jet*. URL: `www.emeraldinsight.com/journals.htm?articleid=1789813&show=html.com`.

[37]   T. L. Schmitz and Smith. *Mechanical vibrations modeling and measurement.* 2012. URL: `http://dx.doi.org/10.1007/978-1-4614-0460-6`.

[38]   M. Schwartz. *Smart materials*. 2009. URL: `http://www.worldcat.org/isbn/9781420043723`.

[39]   D. J. Siler and K. B. J. Demoret. "Variable stiffness mechanisms with SMA actuators". *Smart Structures and Materials 1996*. Vol. 2721. 1. The International Society for Optical Engineering., 1996, pp. 427–435. DOI: `10.1117/12.239158`.

[40]   B. L. Smith and A. Glezer. "The formation and evolution of synthetic jets". *Physics of Fluids* 10.9 (1998), pp. 2281–2297. DOI: `10.1063/1.869828`.

[41]   Sumer and J. Fredsøe. *Hydrodynamics around cylindrical structures*. World Scientific, 1997. ISBN: 9810228988.

[42]   S. Ugrina and A. B. Flatau. "Investigation of synthetic jet actuator design parameters". *Smart Structures and Materials 2004*. Vol. 5390. 1. The International Society for Optical Engineering., 2004, pp. 284–296. DOI: `10.1117/12.547541`.

[43]   T. Vekve. "An experimental investigation of draft tube flow". PhD thesis. NTNU, 2004.

[44]  I. K. Vilberg. "Use of Flow Control on the Leading Edge for Performance Enhancement and Mitigation of Sources of Noise and Vibration". MA thesis. NTNU, 2010.

[45]  P. L. Walsh and J. S. Lamancusa. "A variable stiffness vibration absorber for minimization of transient vibrations". *Journal of Sound and Vibration* 158.2 (1992), pp. 195–211. DOI: 10.1016/0022-460X(92)90045-Y.

[46]  Z. Wei, P. H. Finstad, G. Olimstad, E. Walseth, and M. Eltvik. "High Pressure Hydraulic Machinery (Compendium, EP8407)". 2009.

[47]  F. M. White. *Fluid Mechanics.* Sixth. McGraw-Hill, 2008. ISBN: 978-0-07-128645-9.

[48]  M. M. Zdravkovich. "Review and classification of various aerodynamic and hydrodynamic means for suppressing vortex shedding". *Journal of Wind Engineering and Industrial Aerodynamics* 7.2 (1980).

[49]  P. Zhang, J. Wang, and L. Feng. "Review of zero-net-mass-flux jet and its application in separation flow control". *Science in China Series E: Technological Sciences* 51.9 (2008), pp. 1315–1344. DOI: 10.1007/s11431-008-0174-x.

# Appendix A

# RANS solvers and turbulence modelling

*This section has previously been published in the appendix of this author's project thesis.*

ANSYS Fluent is a RANS solver, where RANS refers to Reynold Averaged Navier-Stokes. Reynolds averaging is a technique for solving the Navier-Stokes equations when velocity is expressed in terms of the sum of a mean and a fluctuating velocity component:

$$\vec{u} = \vec{U} + \vec{u'} \tag{A.1}$$

Replacing $\vec{u}$ in the Navier-Stokes equations gives six new unknowns; the so-called Reynolds stresses for which no equations exist. Therefore, models for the stress terms are required. The Boussinesq approximation relates Reynolds stresses to turbulent viscosity $\nu_t$.

Turbulence viscosity is modelled by turbulence models. Among the most popular are the two equation models $k - \epsilon$ and $k - \omega$. Both models are based on the Boussinesq approximation. In $k - \epsilon$ and $k - \omega$ models, turbulent viscosity depends on two parameters ($k$ and $\epsilon$ and $k$ and $\omega$, respectively). For the SST $k - \omega$ model, transport equations are given below in Eqns. A.2 and

A.3. The equations are found in *ANSYS FLUENT Theory Guide* [4].

$$\frac{\partial}{\partial t}(\rho k) + \frac{\partial}{\partial x_i}(\rho k u_i) = \frac{\partial}{\partial x_j}\left(\Gamma_k \frac{\partial k}{\partial x_j}\right) + \tilde{G}_k - Y_k + S_k \qquad (A.2)$$

$$\frac{\partial}{\partial t}(\rho \omega) + \frac{\partial}{\partial x_j}(\rho \omega u_j) = \frac{\partial}{\partial x_j}\left(\Gamma_\omega \frac{\partial \omega}{\partial x_j}\right) + G_\omega - Y_\omega + D_\omega + S_\omega \qquad (A.3)$$

| | |
|---|---|
| $\tilde{G}_k$ | Generation of turbulence kinetic energy due to mean velocity gradient |
| $G_\omega$ | Generation of $\omega$ |
| $\Gamma_k, \Gamma_\omega$ | Effective diffusivity of $k$ and $\omega$ |
| $Y_k, Y_\omega$ | Dissipation of $k$ and $\omega$ due to turbulence |
| $D_\omega$ | Cross-diffusion term |
| $S_k, S_\omega$ | Source terms |

# Appendix B

# UDF C-code

The following code is used as input for the moving piston wall in all CFD simulations. Variables `freq` and `amp` are altered to obtain an array of different operation points.

```
#include"udf.h"
DEFINE_GRID_MOTION(synjet,domain,dt,time,dtime)
{
Thread *tf = DT_THREAD(dt);
face_t f;
Node *v;
real NV_VEC(axis);
real displ;
real freq=1;
real amp=0.02;
int n;
displ=-dtime*2*3.14*freq*amp*sin(2*3.14*freq*time);
NV_D(axis, =, 0.0, 1.0, 0.0);

begin_f_loop(f,tf)
{
f_node_loop(f,tf,n)
{
```

```
v = F_NODE(f,tf,n);
/* update node if the current node has not been
previously visited when looping through previous faces */
if ( NODE_POS_NEED_UPDATE (v))
{
/* indicate that node position has been updated
so that it's not updated more than once */
NODE_POS_UPDATED(v);
NV_V_VS(NODE_COORD(v), =, NODE_COORD(v), +, axis,*,displ);
}
}
}
end_f_loop(f,tf);
}
```

# Appendix C

# Hints on loading and compiling UDFs in Fluent

In order to run a UDF C-code in Fluent, a compiler needs to be downloaded and configurated. It is not necessarily a straightforward task to make Fluent and the compiler co-operate correctly.

ANSYS Support has published an instructive note which is essential for loading and compiling UDFs on NTNU computers, where a free C compiler needs to be downloaded. The following page displays a copy of their suggestion.

## Compiling and Loading FLUENT 64-bit UDFs using the "FREE" Microsoft Visual Studio 2010 32-bit Express Edition and the 7.0 SDK

**IMPORTANT SUPPORT NOTE**: The 2010 Express Edition and the SDK will allow you to compile 64-bit UDFs for FLUENT. **However, the installation and use of the Express and the SDK is not "officially" supported so we ask that you get your IT folks involved in the actual installation.** Also, you **CANNOT** compile UDFs for FLUENT without first opening the SDK Command prompt window and starting FLUENT from this window.

### Instructions

1. Download the Microsoft Visual Studio Express Edition (2010) performing a default installation http://www.microsoft.com/express/Downloads/#2010-Visual-CPP
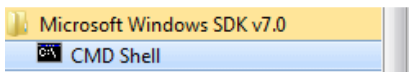
### 7.0 SDK

### Microsoft Windows SDK for Windows 7 and .NET Framework 3.5 SP1

http://www.microsoft.com/downloads/en/confirmation.aspx?familyId=c17ba869-9671-4330-a63e-1fd44e0e2505&displayLang=en

### Starting FLUENT using the SDK 7.0 Command Prompt Window

1. Open up the SDK Command Window. This is required as this will set the compiler environment variables.



2. Launch FLUENT 13.x from this window.
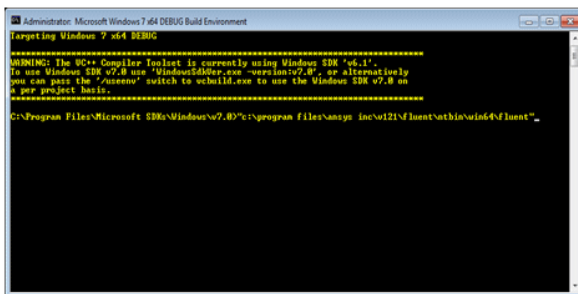


New udf.bat file required for compiling FLUENT 13 and using the 2010 Compiler

The Microsoft Visual Studio 2010 Professional Edition Compiler is not officially supported. In order to compiler UDFs using this compiler you will need to download a modified udf.bat file

**In C:\Program Files\ANSYS Inc\v130\fluent\ntbin\win64** rename the original udf.bat to original-udf.bat. Replace it with the one downloaded and rename the downloaded file, **udf.bat** to the same directory. You can locate this udf.bat file by choosing this link.

http://www.fluentusers.com/support/installation/winfaq/udfguidenetp2010FL13.htm